10,11,05

Phase transitions in frustrated Ising models (Review)

© A.K. Murtazaev, M.K. Ramazanov

Institute of Physics, Dagestan Federal Research Center, Russian Academy of Sciences, Makhachkala, Russia

E-mail: sheikh77@mail.ru

Received June 18, 2023
Revised June 23, 2023
Accepted June 24, 2023

The current state of research on phase transitions and critical phenomena in frustration is considered modeled Ising models. The results obtained on the basis of highly efficient algorithms are discussed. Monte Carlo method for Ising models on lattices of various dimensions and types. A main attention given to the results of studying phase transitions, critical and thermodynamic properties of models Ising, taking into account the exchange interactions of the first and second neighbors, as well as the external magnetic fields. Phase diagrams of the dependence of the critical temperature on the value of the exchange interactions of second neighbors and an external magnetic field. The regions of observation of phase transitions of the first and second kind. The universality classes of critical behavior are established. For some models have ranges with non-universal critical behavior. Discussed features of the critical behavior of frustrated Ising models.

Keywords: Ising model, frustrations, phase transitions, Monte Carlo method.

DOI: 10.61011/PSS.2023.09.57102.114

Content

1. Introduction

The Ising model is the most simple and frequently used model for the study of cooperative phenomena in statistical mechanics. The Ising model was offered and used for the first time by Lenz [1] and Ising [2]. In 1925 Ising found a solution for a one-dimensional chain case, though the solution did not cover a phase transition (PT) (PT in an atomic lattice occurs at $T = 0$) [2]. Almost 20 years had passed until Lars Onsager published the solution for a two-dimensional case without external field and proved that PT can exist in two-dimensional systems [3]. Despite multiple attempts taken by researchers, no accurate solution for the tree-dimensional Ising model has been found yet.

The Ising model was initially used for theoretical description of the magnetic PT in ferromagnetic materials. Being one of the few accurately solved models, it is now used as a reference for verification of new theories, approximations and numerical algorithms. During many years, the Ising model has been considered as a mathematical model. However, experimental implementations of the Ising model have been found in magnetism. Currently, there are numerous magnetic materials, some of whose properties may be successfully described by the Ising model. They include, for example, fluorides (MnF_2, FeF_2 etc.). Theoretical description of the critical behavior of these compounds in accordance with the Ising model is in good agreement with the applicable experimental data. (Fluorides, although having the Ising anisotropy, exhibit also the „Heisenberg“ properties — for example, the have magnon excitations that are absent in the Ising model).

In addition to traditional applications in magnetism, the Ising model is used in many applications closely connected with cooperative phenomena in various research areas. The Ising model and its versions have proven to be useful in statistical physics for PT order-disorder modelling in metal alloys, liquid-gas transition and liquid mixtures [4–6]. The Ising models are also successfully used to study various collective phenomena in physics [7]. The Ising model have been used in medicine, because it allows to simulate

tumor growth or electromechanical alternations of the heart cells [8,9]. The Ising model applications listed above are certainly not limited. Nevertheless, this list demonstrates the flexibility of models similar to the Ising model for the study of a lot of various phenomena and systems.

When describing critical phenomena (CP) in lattice systems, various Ising model versions are used most often. They were used as the basis to get comprehensive information about the behavior of various thermodynamic values in a wide temperature range and other physical property ranges. The investigations have been carried out using various types and spatial dimensions of lattices, as well as with varying numerous parameters. Lately, the computational physics (CP) methods have been extensively used to study also a critical region with calculation of critical indices (CI), and the achieved accuracy is not lower, but is often higher than the best results achieved by other methods [10–12].

Currently, the center of gravity of theoretical research has moved towards more realistic Ising models including numerous factors inherent in real crystals and not considered in first approximation models. Such factors include: anisotropy, impurities, vs, lattice vibrations, frustrations, etc. [13,14]. Investigations of complex magnetic structures such as highly frustrated magnetic compounds and metallic nanosystems, spin glasses, spin ice, amorphous and nanogranulated materials and multilayer nanofilms play an important role in the modern condensed matter physics [15–17]. Physical properties of frustrated spin systems differ greatly from the corresponding systems without frustrations. The nature of PT, magnetic structures of the ground state, critical and thermodynamic properties of frustrated spin systems depend on many external factors. The presence of frustrations in the system may result in new physical behavior. Investigation of the effect of frustrations on PT, thermodynamic, magnetic and critical properties of spin systems gave a lot of interesting results [18,19]. Despite the achieved success, several issues related to PT, critical, thermodynamic and magnetic properties of frustrated spin systems still remain open.

The objective of the study is to summarize the findings of investigations of PT, critical, magnetic and thermodynamic properties of frustrated spin systems described by the Ising model. The results frustrated Ising model investigations carried out using the Monte Carlo (MC) method are reviewed herein mostly using the publications of the authors of this summary. Our findings are compared with the literature data.

The Ising model and results of its investigations are discussed in Section 2. Section 3 describes the frustration effects in the Ising models. The impact of frustrations on the Ising model behavior is discussed. Numerical investigations of PT, magnetic and thermodynamic properties are discussed in Section 4. This section describes the triggering conditions and impact of frustration on the physical properties of the Ising model for various types of lattices and dimensions. Section 5 gives the numerical experiment results obtained for the Ising models in the external magnetic field. The conclusion contains a summary of findings.

2. Ising model

In the Ising model, spins are located in d-dimensional lattice sites. Variable spin models may have only two values ($+1$ or -1) and correspond to two possible spin orientations (upwards or downwards).

The Ising model Hamiltonian may be represented as follows:

$$H = -\frac{1}{2} J \sum_{i,j} S_i S_j - h \sum_i S_i, \qquad (1)$$

where J is the exchange interaction parameter between spins i and j, h is the external magnetic fields and $S_i = \pm 1$ for all i.

Despite the relative simplicity of the Ising model, until now only two particular cases with dimensions $d = 1$ and $d = 2$ have been solved accurately [20]. These accurate solutions help estimate the suitability of the approximate methods used to study 3D models. Moreover, these models may serve as a good approximation for some real physical systems, because there is a large class of magnetic and non-magnetic materials, which can be classified as one-dimensional or two-dimensional.

It should be noted that no solution or the three-dimensional Ising model case has been found yet. Therefore, the study of the Ising model, in particular by the numerical experiment methods, is of great interest. The MC method has been first used to calculate the energy and magnetization of the two-dimensional Ising model with nearest-neighbor interaction [21]. This calculation reproduces Onsager's accurate result for energy with an error within 1% in a wide range, excluding the direct critical point region. The square lattice and simple cubic lattice Ising models were studied in detail as early as in the 1970s [22–25]. In [24,25], the MC method was used to study the simple lattice Ising model with periodic boundary conditions (PBC) and free surfaces, where rather detailed information was obtained regarding the effects connected with the small size of the lattice of interest. The free surface effect on the system properties is also discussed. In [25], strong dependence of energy, magnetization and susceptibility on the linear dimension of the system has been found. When superimposed on the PBC system, these dependences are reported to be lower, moreover, the order parameter in the low-temperature region does not depend on the system size.

In the next years, the focus has shifted towards the study of models with complex type interactions and on other classes of lattices. The number of such investigations is large with only some of them described below. The Ising model has been further studied with anisotropy (the Ising model where spins have higher values) [26–29], with biquadratic interaction [30], in random fields [31,32], in

magnetic fields [33–35], in transverse field [36], with three-spin interaction [37], with four-spin interaction [38], in antiferromagnetic systems [39–44], with frustration [45–56], with mixed spin value [57–60], with exchange interaction competition [61–69], on decorated lattices [59,60,70,71]. The Ising model in various dimensions was studied in detail in [11], where one of latest and most accurate results have been obtained for two-, three- and five-dimensional cases. The basic aspects of various algorithms and applications of finite-size scaling (FSS) are also provided. These investigations were used to obtain comprehensive information about the Ising model. Thus, short- and long-range order parameters, internal energy, heat capacity, other thermodynamic parameters, CI for the Ising model and its various versions were calculated.

3. Frustrations in the Ising model

Term „frustrution“ was first used by Toulouse in the theory of magnetism in 1977 [72]. Frustrations in the condensed matter physics generally mean an event when simultaneous minimization of all Hamiltonian summands is impossible in the presence of competing interactions. This causes strong degeneracy of the ground state of a system with nonzero entropy at zero temperature. Frustration in the system may be caused by the exchange interaction competition or specific lattice geometry.

Consider three random spins interacting with each other (Figure 1) and assume that the interactions are equal to each other, but may have opposite signs. When all three interaction constants J_{12}, J_{23} and J_{13} are positive or two of them are negative (i. e. when the product of interactions along the triangle is positive), then the ground state (energy minimum) of this three-spin system will be the only one (with accuracy up to the total sign reversal of all three spins) (Figure 1, *a*). However, when the product of interactions along the triangle is negative (one of the interactions is negative, or all three interactions are negative), then the ground state of such system is degenerate. I.e. when we record the first spin up is and go round the triangle setting the spin orientation in accordance with the specified interactions, then last third spin orientation will be uncertain — „up“ state and „down“ state energies will be equal. Figure 1, *b* shows the situation when all three interactions are negative. When the first spin looks up, then in accordance with $J_{12} < 0$ the second spin shall look down, however, after that uncertainty occurs for the third spin: in accordance with $J_{23} < 0$, it shall look up, and in accordance with $J_{13} < 0$, it shall look down. The same ground state degeneracy phenomenon occur in any closed chain consisting of a random number of spins, if the product of spin-spin interactions along the chain is negative. This phenomenon is called frustrations.

Frustrations change the system behavior considerably compared with the corresponding unfrustrated system. In spin systems, frustrations may result tremendous degeneracy of the ground state, i.e. the system may have a great amount of states with low energy close to the ground state energy that, due to their high entropy, may make the final (and even dominating) contribution to thermodynamics even in a low temperature range [73].

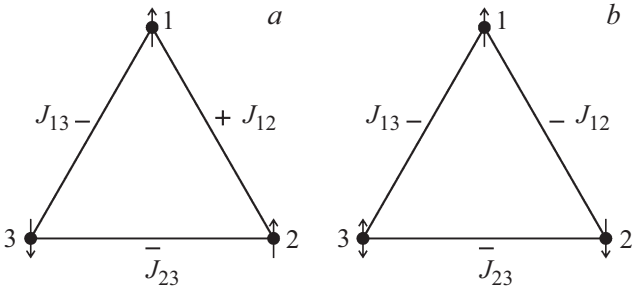

Figure 1. Frustrations in the system of three spins.

Theoretical model of the geometrical frustration offered by Vanier [74] has shown that triangle lattice antiferromagnetic has totally different behavior compared with square lattice antiferromagnetic and has no magnetic order up to zero temperature. Geometrically frustrated antiferromagnetics make a large class of materials, where frustration has a merely structural origin and gives rise to strongly degenerate ground states.

Investigations of PT and CP in frustrated spin systems by traditional theoretical, experimental and numerical methods come across several formidable problems in an attempt to calculate critical parameters, define the features, nature and mechanisms of critical behavior of such systems [75,76]. This is associated with the fact that such models have numerous local energy minima valleys. This and some other reasons have resulted in a situation where PT and CP are now extensively studied by the computational physics methods — MC methods [11,12,77], that ensure successful study of critical properties of systems with complex realistic Hamiltonians in wide temperature and other parameter ranges. But conventional MC methods poorly cope with solution of these problems. Therefore, many new MC method algorithms have been developed lately in order to overcome these problems. Replete algorithms and the Wang–Landau algorithm of the MC method are the most powerful and efficient for investigation PT and CP in frustrated systems [78,79].

4. Phase transitions, magnetic, thermodynamic and critical properties of the frustrated Ising model

4.1. Square lattice Ising model

Two-dimensional Ising model with nearest-neighbor interactions has been well studied by various methods and approaches [2,80–82]. This square lattice model with ferromagnetic first- and second-neighbor interactions has

been accurately solved. However, consideration of antiferromagnetic second-neighbor interactions in the classical two-dimensional Ising model is followed by ground state degeneracy and occurrence of various phases and PT, and affects the critical behavior of the model [83].

In the late 1970s, the first renormalization group calculations and numerical simulation by the MC method for the two-dimensional antiferromagnetic square lattice Ising model with second-neighbor interactions carried out in [84,85]. The authors of the papers mentioned above assumed that a second-kind PT occurs in this model and calculated the PT temperature and CI. In [84–87], it is also shown that the second-kind PT takes place in the antiferromagnetic square lattice Ising model with first- and second-neighbor interactions. In addition, this model may have „abnormal" CI. At the same time, dependence of CI on $r = J_2/J_1$ was found, where J_1 and J_2 are first- and second-neighbor exchange interaction constants, respectively. But the continuous PT scenario has been still in question after the calculations on the basis of the mean-field theory that have shown the existence of the first-kind PT [88]. According to [89–91], the first-kind PT shall be also observed for the square lattice Ising model with the ferromagnetic first-neighbor interactions and antiferromagnetic second-neighbor interactions within $r = 0.5-1.2$. In [92], we found the second-kind PT for the antiferromagnetic square lattice Ising model at $r = 1$.

This Section contains the results obtained using the replete algorithm of the MC method for the antiferromagnetic square lattice Ising model including the first- and second-neighbor interactions. The antiferromagnetic square lattice Ising model including the first- and second-neighbor interactions is described by the following Hamiltonian:

$$H = -J_1 \sum_{\langle ij \rangle} (S_i \cdot S_j) - J_2 \sum_{\langle il \rangle} (S_i \cdot S_l), \qquad (2)$$

where $S = \pm 1$ is the Ising spin. The first term in equation (2) takes into account the first-neighbor exchange interaction ($J_1 < 0$), and the second term takes into account the second-neighbor exchange interaction ($J_2 < 0$). Competition of the first- and second-neighbor exchange interactions induces frustrations in this model. The calculations were carried out for systems with PBC and linear dimensions $L \times L = N$, $L = 20-150$, where L is measured in the lattice cell dimensions. The relation of the second- and first-neighbor exchange interactions varied within $0.0 \le r \le 1.0$.

To determine the temperature behavior of heat capacity and susceptibility, the following expressions were used [93]:

$$C = (NK^2)(\langle U^2 \rangle - \langle U \rangle^2), \qquad (3)$$

$$\chi = \begin{cases} (NK)(\langle m^2 \rangle - \langle |m| \rangle^2), & T < T_N \\ (NK)\langle m^2 \rangle, & T \ge T_N \end{cases}, \qquad (4)$$

where $K = |J|/k_B T$, N is the number of pages, U is the internal energy, m is the order parameter.

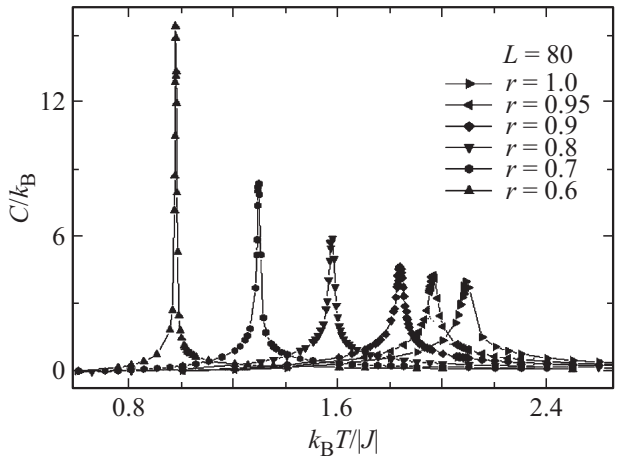

Figure 2. Dependence of heat capacity on temperature for various r.

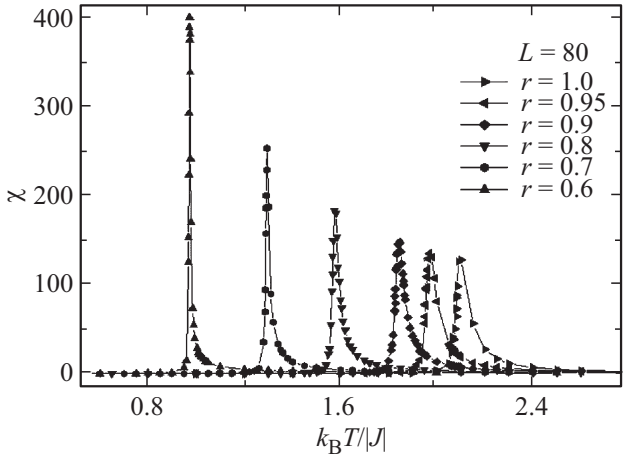

Figure 3. Dependence of susceptibility on temperature for various r.

The order parameter of system m was calculated using the expression [94]:

$$m_\lambda = \frac{4}{N} \sum_{i \in \lambda} S_i, \quad \text{where} \quad \lambda = 1, 2, 3, 4, \qquad (5)$$

$$m^a = [m_1 + m_2 - (m_3 + m_4)]/4, \qquad (6)$$

$$m^b = [m_1 + m_4 - (m_2 + m_3)]/4, \qquad (7)$$

$$m = \sqrt{(m^a)^2 + (m^b)^2}, \qquad (8)$$

where m_1, m_2, m_3, m_4 is the order parameter on sublattices.

Figure 2–5 shows the temperature dependences of heat capacity C and susceptibility χ calculated for $L = 80$ at various r values (hereinafter the statistical error does not exceed the sizes of symbols used to plot the dependences). The figures show that distinct peaks of heat capacity C and susceptibility χ are observed for all r values near the critical temperature. Note that decreasing r within $0.6 \le r \le 1.0$ is followed by the shift of peaks towards

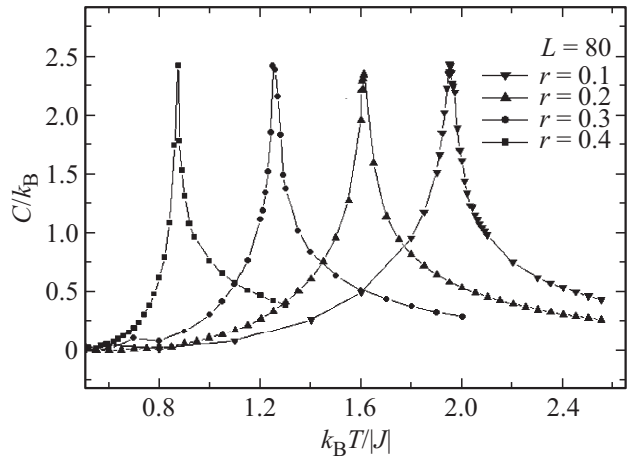

Figure 4. Dependence of heat capacity on temperature for various r.

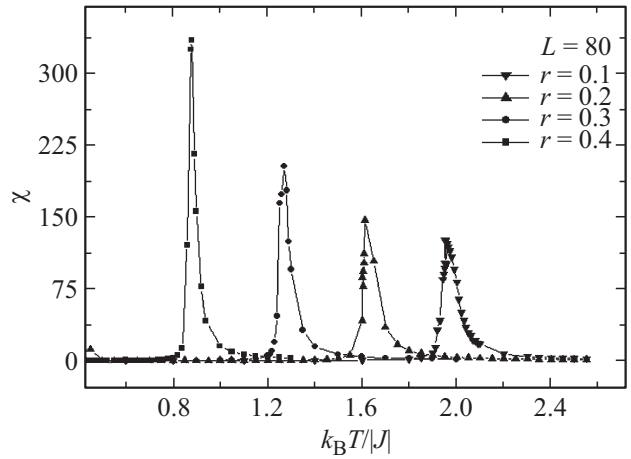

Figure 5. Dependence of susceptibility on temperature for various r.

lower temperatures and the growth of both absolute heat capacity and susceptibility peaks is observed at the same time. An opposite picture is observed within $0.1 \leq r \leq 0.4$. With decreasing r from 0.4 to 0.1, PT temperature moves towards higher temperatures.

To determine the critical temperatures T_N, we used the fourth-order Binder cumulant method U_L. The fourth-order cumulants for magnetization and energy are as follows [95]:

$$U_L = 1 - \frac{\langle m^4 \rangle_L}{3\langle m^2 \rangle_L^2}, \tag{9}$$

$$V_L = 1 - \frac{\langle U^4 \rangle_L}{3\langle U^2 \rangle_L^2}, \tag{10}$$

where U_L is the cumulant for magnetization, V_L is the cumulant for energy.

Expressions (9) and (10) allow to define the critical temperature T_N more accurately. It should be noted that the use of the Binder cumulants also allows good determination of PT in the system. In case of the second-kind PT, the temperature curves of the Binder cumulants U_L are known to have a clearly defined intersection point [95].

Figure 6 shows typical dependences of UL on the temperature at $r = 0.2$ for various L values. This figure shows the determination accuracy of the critical temperature. The detail shows that a clearly defined intersection point is observed in the critical region (hereinafter the temperature is given in terms of $|J|/k_B$), that is indicative of the second-kind PT. Critical temperatures for other r values were also defined in a similar way.

Figure 7 shows the phase diagram of dependence of the critical temperature on the second-neighbor interaction. The diagram shows that T_N for $r = 0.5$ has the minimum value. This is due to the fact that a frustrated state occurs near $r = 0.5$ in the system for the model of interest. The presence of frustrations is confirmed by the behavior of the temperature dependence of heat capacity shown in Figure 8. This figure shows that the heat capacity near the frustration point $(r = 0.5)$ has no sharp peak and a spreading trend

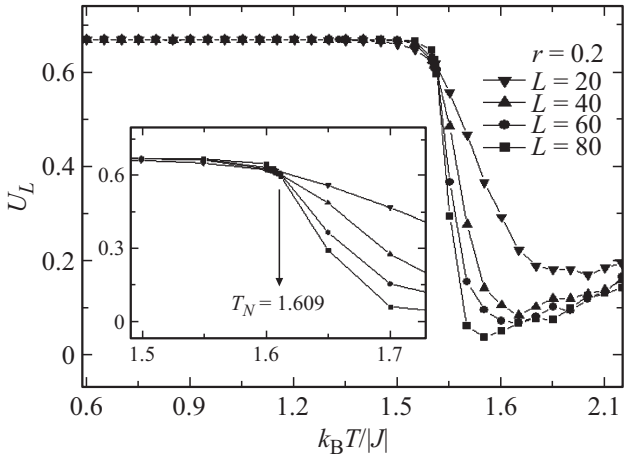

Figure 6. Dependences of the Binder cumulant on temperature for $r = 0.2$ at $L = 20$, 40, 60 and 80.

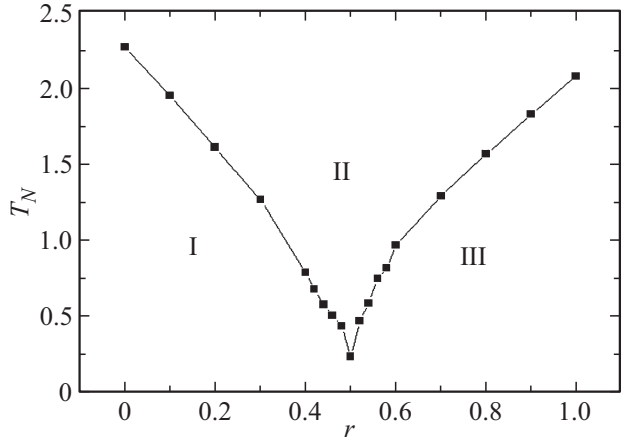

Figure 7. The phase diagram of dependence of the critical temperature on the second-neighbor interaction for the two-dimensional square lattice Ising model.

Table 1. Critical parameter values for the square lattice Ising model

r	T_N	ν	α	β	γ	η	$\alpha + 2\beta + \gamma = 2$
1.0	2.081(1)	0.830(1)	0.35(1)	0.09(1)	1.45(1)	0.25(1)	1.98
0.95	1.955	0.82	0.36	0.09	1.44	0.24	1.98
0.9	1.829	0.80	0.41	0.09	1.43	0.22	2.02
0.8	1.567	0.78	0.46	0.10	1.37	0.24	2.03
0.7	1.289	0.74	0.51	0.10	1.28	0.26	1.99
0.4	0.873	1.01	0.01	0.11	1.75	0.25	1.98
0.3	1.258	0.99	0.01	0.12	1.76	0.23	2.01
0.2	1.612	0.99	0.01	0.11	1.76	0.23	1.99
0.1	1.952	1.01	0.01	0.12	1.76	0.26	2.01
0.0	2.268	1	0.01	0.13	1.75	0.25	2.02
$r = 0.0$ [94]	2.262	1	0	0.125	1.75	–	2

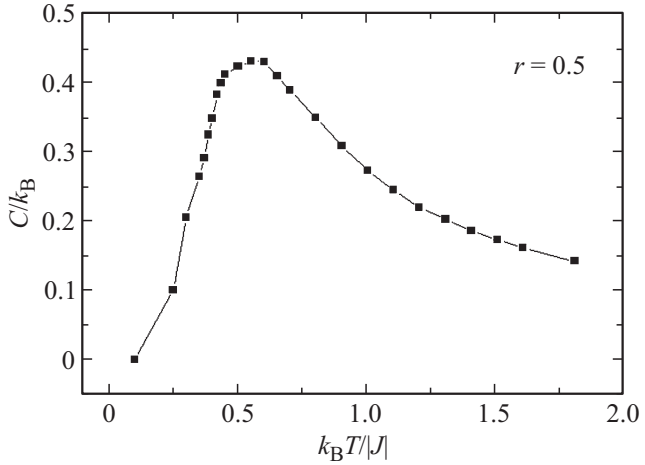

Figure 8. Dependence of heat capacity on temperature for $r = 0.5$ at $L = 150$.

is observed. Such heat capacity behavior is typical for frustrated systems. The diagram shows that near point $r = 0.5$ three different phases intersect: I — ferromagnetic, II — paramagnetic and III — superantiferromagnetic (collinear antiferromagnetic structure).

Review of our findings shows that the second-kind PT is observed within $0.0 \le r \le 1.0$, except for $r = 0.5$ and $r = 0.6$. histogram data analysis also supports this. Figure 9 shows the energy distribution histogram for $r = 0.2$. The curve is plotted near the critical point for lattice $L = 150$. The figure shows one peak, which is typical for the second-kind PT [79]. Similar behavior is observed on the histograms for all r values within the interval, except $r = 0.6$. It is shown that near point $r = 0.5$ the system becomes fully frustrated and two peaks are observed on the histogram for $r = 0.6$, which is typical for the first-kind PT. The authors of [96] found the second-kind PT within $r < 0.5$. However, the results of this study show that the first-kind transition is observed in $0.5 < r < 0.948$. The data obtained in [96] partially coincide with our findings. Findings of later investigations showing that this model demonstrates the second-kind PT within $0.0 \le r \le 0.4$ and $0.67 \le r \le 1.0$ fully correspond to our data [97,98].

To calculate static CI of heat capacity α, susceptibility γ, magnetization β and correlation radius ν, the FSS theory ratios were used. According to the FSS theory, the following expressions are satisfied in the system with dimensions $L \times L$ at $T = T_N$ and rather high L [99–102]:

$$m \sim L^{-\beta/\nu}, \tag{11}$$

$$\chi \sim L^{\gamma/\nu}, \tag{12}$$

$$V_n \sim L^{1/\nu} g_{V_i}, \tag{13}$$

where g_{V_i} is the constant, and V_i may be as follows

$$V_i = \frac{\langle m^i E \rangle}{\langle m^l \rangle} - \langle E \rangle, \ (i = 1, 2, 3, 4), \tag{14}$$

These expressions were used to calculate β, γ and ν.

For approximation of the temperature dependence of heat capacity on L, the following expression was used [101,103,104]:

$$C_{\max}(L) = C_{\max}(L = \infty) - \alpha L^{\alpha/\nu}, \tag{15}$$

where a is some coefficient.

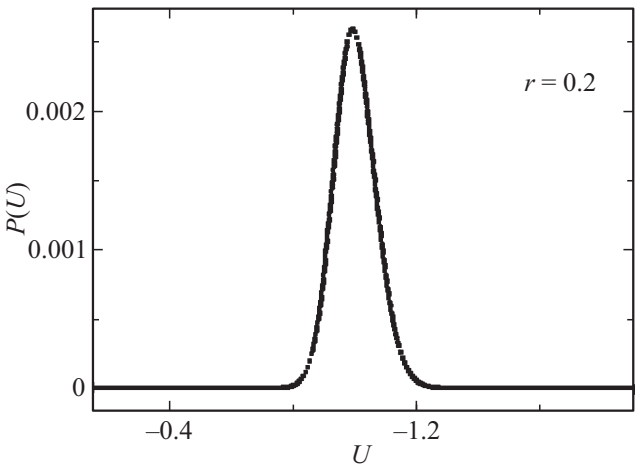

Figure 9. Energy distribution histogram for $r = 0.2$.

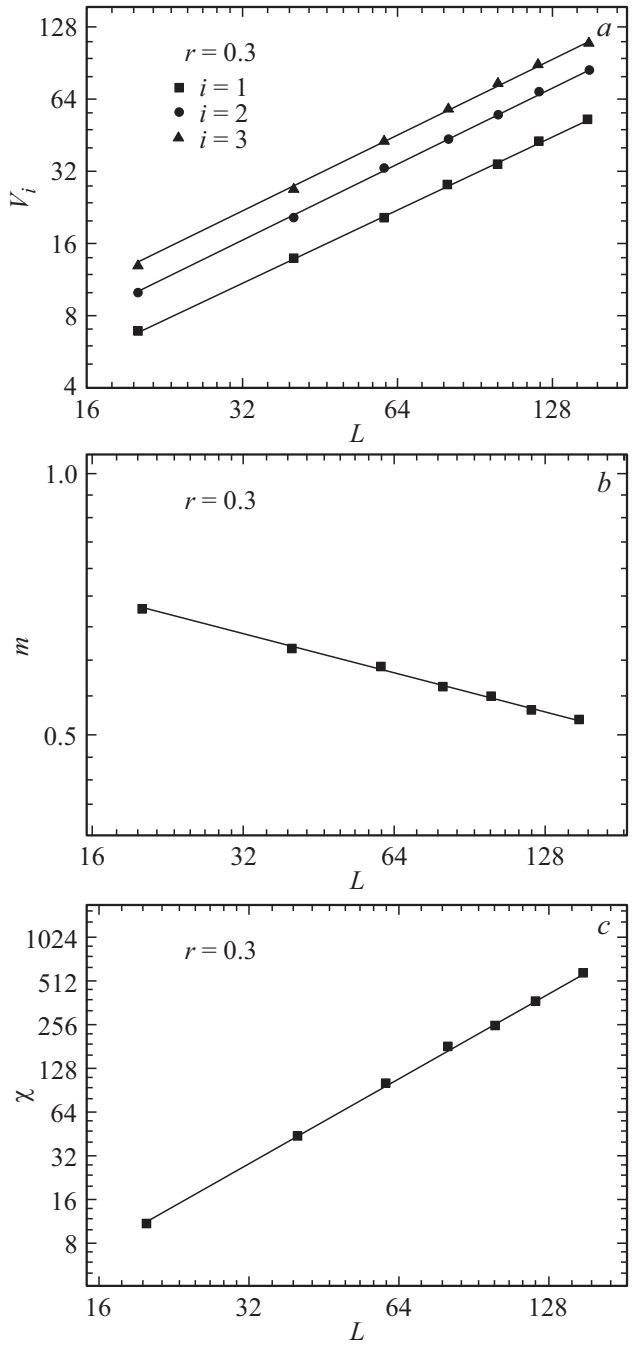

Figure 10. Dependence of V_i, order parameter m and susceptibility χ on the linear lattice dimensions L for $r = 0.3$.

Critical parameters were calculated for $0.0 \le r \le 0.4$ and $0.7 \le r \le 1.0$, where, according to our data and data obtained by other authors, this model demonstrates the second-kind PT [97,98].

Figure 10 shows typical dependences of V_i, magnetic order parameter m and susceptibility χ on the linear lattice dimensions L in log-log scale for $r = 0.3$. The inclinations of the lines define $1/\nu$, β/ν and γ_ν values. This scheme was used to determine the heat capacity α/ν. Having the data for ν, static CI α, β and γ were calculated. This procedure was used to calculate CI for $r = 1$, 0.95, 0.9, 0.8, 0.7, 0.4, 0.3, 0.2, 0.1 and 0. All static CI values calculated in this way are listed in Table 1.

The procedure used by us to determine the Fisher index η shall be particularly emphasized. Using the relation of susceptibility χ and correlation radius χ [105]:

$$\chi \propto \xi^{\gamma/\nu}, \tag{16}$$

as well as $\eta = 2 - \gamma/\nu$ correlating η and ν, we get

$$\ln(\chi/\xi^2) = c - \eta \ln \xi, \tag{17}$$

where c is some constant. For systems with finite dimensions $\xi = L$. Then, for $T = T_N$, we have

$$\ln(\chi/L^2) = c - \eta \ln L. \tag{18}$$

The Fisher index values calculated in this way are also listed in Table 1. Comparison of numerical CI values calculated herein with the literature data [94] (for $r = 0.0$) shows their good agreement. CI of heat capacity $\alpha = 0.342\,(5)$, order parameter $\beta = 0.103\,(3)$, susceptibility $\gamma = 1.451\,(7)$ and correlation radius $\nu = 0.84\,(1)$ calculated in [94,106] coincides within the allowable accuracy with our data at $r = 1$. It should be noted that scaling relations are also satisfied well enough for our data showing that CI are calculated with good accuracy [107–110].

As shown in the Table, the critical temperature T_N decreases with decreasing second-neighbor interaction up to $r = 0.4$. With further decrease in r, the critical temperature starts growing. Numerical CI values listed in the Table show that all CI within $0.7 \le r \le 1.0$ change with varying r. Within $0.0 \le r \le 0.4$, all indices coincide with Onsager's data and do not depend on r.

Thus, we can suggest that the critical behavior universality class of the Ising model taking into account the antiferromagnetic second-neighbor interactions is maintained within $0.0 \le r \le 0.4$. Table 1 shows that the model of interest has two regions, which are characterized by different critical behavior. It can be claimed that the change of the second-neighbor interaction results in non-universal critical behavior within $0.7 \le r \le 1.0$.

4.2. Kagome lattice Ising model

Spin systems having the Kagome lattice may be highly frustrated due to the specific geometry. With decreasing temperature, the ordering process in such systems is much slower as compared with even conventional frustrated systems. This behavior is due to the fact that systems with a smaller coordination number can have not only states with non-trivial global degeneracy, but also locally degenerate states [111,112]. When considering exchange interactions only between the nearest neighbors, PT to the magnetically ordered state is not implemented at any finite temperatures. Consideration of the second-neighbor exchange interactions partially releases the degeneracy and

may result in the occurrence of the long-range order and PT at non-zero temperatures [113]. Nevertheless, since the frustration effects are still present, the structure ordering and stabilization process is much slower compared with unfrustrated systems [114].

The two-dimensional Kagome lattice Ising model is one of the extensively studied frustrated models over the last years [115]. This model is an exemplary geometrically frustrated system. In this model with the nearest-neighbor interactions in the ground state, the entropy per spin is non-zero [116]. Spin ordering and long-range order in such system are suppressed due to the fruxtration effects. However, consideration of the second-neighbor interactions stabilizes the ordered spin state and the system reveals PT [114,115].

Two-dimensional antiferromagnetic Kagome lattice Ising model with the first- and second-neighbor interactions is considered. The interest in this model is caused by the fact that it can be used to describe real materials and compounds [116–118]. It is shown in [118] that magnetic ions of Fe^{3+} form the Kagome lattice in plane c in $MFe_3(OH)_6$ family $(SO_4)_2$ ($M = H_3O$, Na, K, Rb, Ag, NH_4, Tl, Pb, Hg) with the mineralogical name „jarosites“. According to the experimental data, interactions between the nearest spins inside and between layers are antiferromagnetic [119]. Since the adjacent layers with Fe^{3+} in jarosites are separated by nonmagnetic ions S, O, K and OH, interplanar exchange is considerably lower than the intraplanar exchange. In addition, PT in the Kagome lattice Ising systems are known to be possible only in case of the ferromagnetic second-neighbor interaction [120].

The antiferromagnetic Kagome lattice Ising model including the first- and second-neighbor interactions is described by the following Hamiltonian:

$$H = -J_1 \sum_{\langle i,j \rangle} (S_i \cdot S_j) - J_2 \sum_{\langle i,l \rangle} (S_i \cdot S_l). \qquad (19)$$

The first term in equation (19) takes into account the antiferromagnetic nearest-neighbor exchange interaction $J_1 < 0$, and the second term takes into account the second-neighbor ferromagnetic interaction $J_2 > 0$. The case of $J_1 = -1$ and $J_2 = 1$ is addressed herein.

To study this model, we used the Wang–Landau algorithm of the MC method. The calculations were carried out for the systems with PBC and linear dimensions $L = 12-120$, the number of particles in the system was equal to $N = 3/4 \times L \times L$.

Expressions relations (3), (4) were used to observe the temperature behavior of the heat capacity and susceptibility. The system order parameter was calculated using the expression [114]:

$$m = \frac{1}{3}\Big(|m_1| + |m_2| + |m_3|\Big), \qquad (20)$$

where m is the sublattice magnetization.

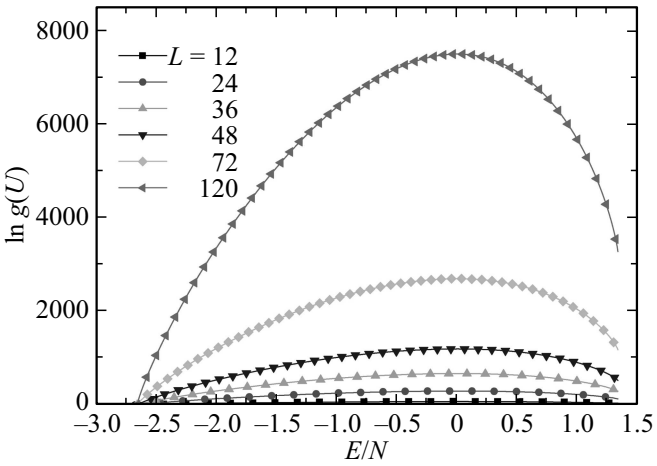

Figure 11. Energy state density $g(E)$ for systems with various linear dimensions L for the two-dimensional Ising model.

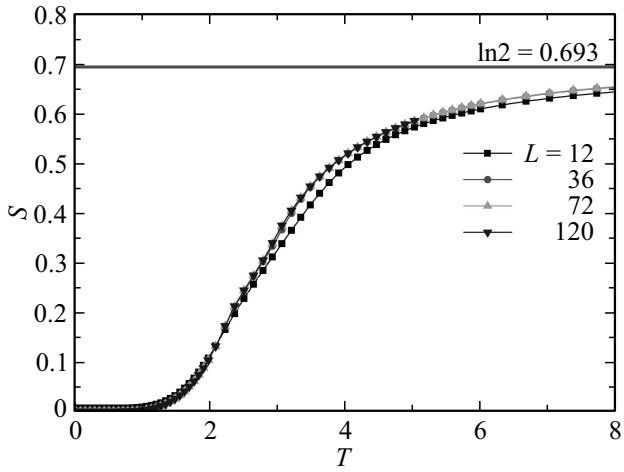

Figure 12. Temperature dependences of entropy.

Energy state density $g(E)$ for systems with various linear dimensions L is shown in Figure 11. The curve shows that there is no ground state degeneracy in this system. We suppose that this is due by the fact that this model addresses the second-neighbor exchange interaction that can facilitate degeneracy removal.

Temperature dependences of entropy S at various linear dimensions of the system are shown in Figure 12. This figure shows that the system entropy with increasing temperature tends to the theoretically predicted value $\ln 2$. At low temperatures near absolute zero, the system entropy tends to zero, while for this model with only nearest-neighbor interactions, the entropy tends to a non-zero value. Such entropy behavior is indicative of considerable influence of the second-neighbor interaction on the thermodynamic properties of the model.

Figures 13 and 14 show temperature dependences of heat capacity and susceptibility obtained at various linear dimensions of the system. It should be noted that both

for heat capacity and susceptibility, unusual behavior is observed which is characterized by the presence of the twin peak. The curves show that the growth of absolute heat capacity and susceptibility peaks is observed with the increasing linear dimensions of the lattice. And the two-peak structure becomes more distinct. Such behavior is associated with the first-neighbor and second-neighbor competition. It can be assumed that the first peak on the curves is caused by the system transition from the ordered state to a partially disordered stated and the second peak corresponds to the system transition to the paramagnetic state.

Temperature dependences of the order parameter m at various linear dimensions of the system are shown in Figure 15. The figure shows that unusual behavior of the order parameter is observed on the curves. These features correspond to the same temperatures at which two peaks were observed on the heat capacity and susceptibility curves (Figures 13 and 14). Such order parameter behavior is obviously associated with the competition of exchange interactions in the system.

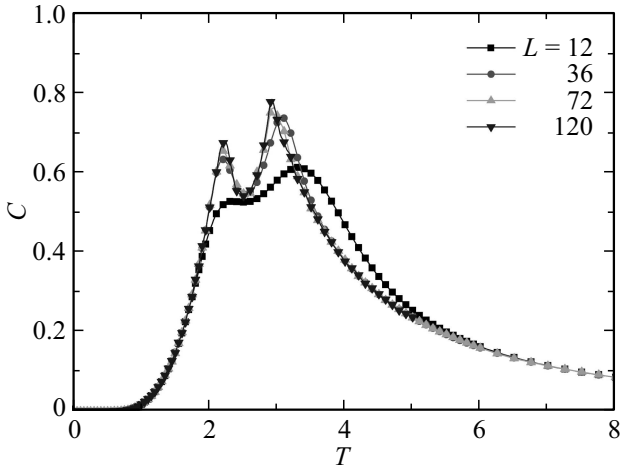

Figure 13. Temperature dependences of heat capacity.

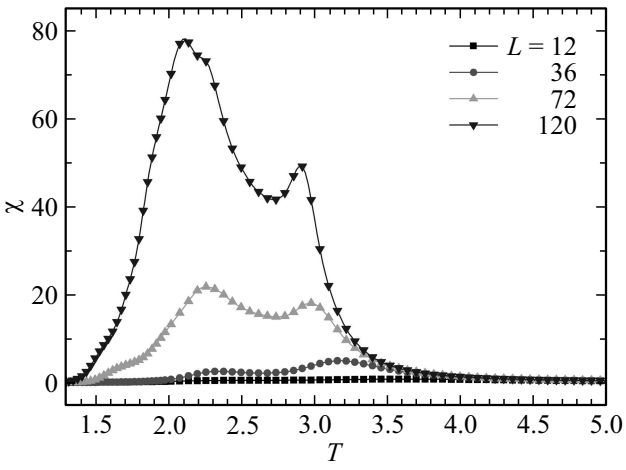

Figure 14. Temperature dependences of susceptibility.

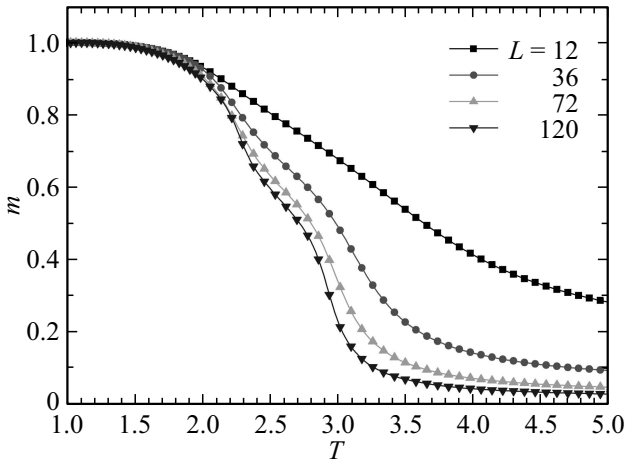

Figure 15. Temperature dependences of order parameter.

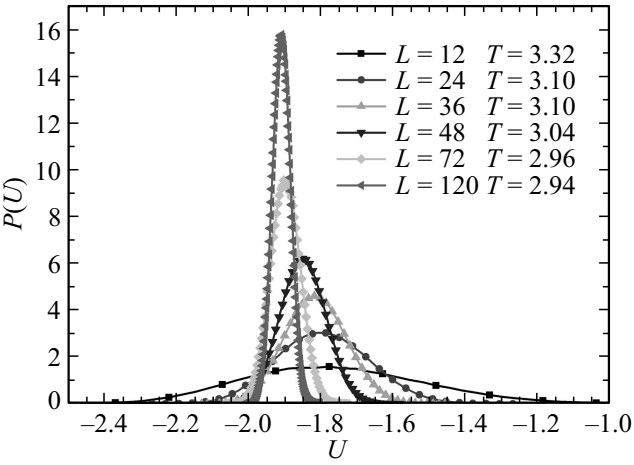

Figure 16. Energy distribution histograms.

Figure 16 shows the energy distribution histograms for systems with different linear dimensions. The curves are plotted near the point corresponding to the temperature of the second heat capacity peak. Since the temperatures of the heat capacity peaks are different for the systems with different linear dimensions, the temperatures corresponding to the peaks are shown on the curves. All histograms are standardized in such a way that the integral of it (integrated probability of all energy states) is equal to one. The curves show a single peak, which is typical for the second-kind PT [94,121,122]. The data analysis suggests that consideration of the ferromagnetic second-neighbor interactions in the two-dimensional antiferromagnetic Kagome lattice Ising model results in the occurrence of the second-kind PT and facilitates unusual behavior of thermodynamic parameters in their temperature dependence [123].

4.3. Simple cubic lattice Ising model

This Section describes the investigations of PT of the antiferromagnetic cubic lattice Ising model taking into

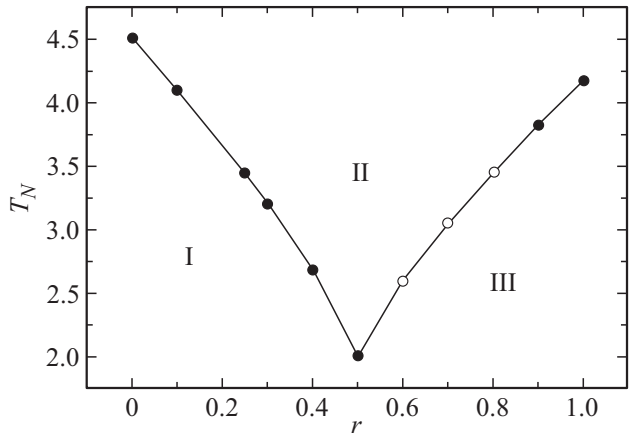

Figure 17. The phase diagram of dependence of the critical temperature on the second-neighbor interaction for the cubic lattice Ising model.

account the second-neighbor interactions inside the layers within $0.0 \le r \le 1.0$. This model is a particular case of the model studied in [124,125], when the second-neighbor interaction between the layers is equal to zero.

The antiferromagnetic cubic lattice Ising model including the first- and second-neighbor interactions is described by the following Hamiltonian:

$$H = -J_1 \sum_{\langle i,j \rangle} (S_i \cdot S_j) - J_2 \sum_{\langle i,l \rangle} (S_i \cdot S_l). \qquad (21)$$

The lattice contains two-dimensional square layers folded along the orthogonal axis. The first term in equation (21) characterizes the antiferromagnetic interaction of all nearest neighbors, whish is assumed equal both inside and between the layers ($J_1 < 0$). The second term characterizes the antiferromagnetic second-neighbor interaction in the same layer ($J_2 < 0$). Consideration of the antiferromagnetic second-neighbor interaction causes frustration in this model.

To study this model, we used the replete exchange algorithm of the MC method. The calculations were carried out for the systems with PBC and linear dimensions $L \times L \times L = N$, $L = 30-90$.

The order parameter of system m was calculated using expression (6)–(8). m_λ was calculated as follows

$$m_\lambda = \frac{4}{N} \sum_{i \in \lambda} (-1)^z S_i, \qquad (22)$$

where z is the number of the lattice layer.

To determine the critical temperature T_N for all r values, the method of the fourth-order Binder cumulants U_L was used.

Figure 17 shows the phase diagram of dependence of the critical temperature on the second-neighbor interaction. This diagram shows that three different phases intersect near point $r = 0.5$: antiferromagnetic — I, paramagnetic — II and superantiferromagnetic (collinear) — III. Magnetic structure of the ground state of the superantiferromagnetic phase was addressed in detail in [126], and magnetic structures of the antiferromagnetic and paramagnetic phases are well known.

We considered transitions from the antiferromagnetic phase to the paramagnetic phase and from the superantiferromagnetic phase to the paramagnetic phase. We did not address the transition from the antiferromagnetic phase to the superantiferromagnetic phase. We suggest that there is a coexistence region for both phases at the phase boundary.

The diagram shows that within $0.0 \le r \le 0.5$ transition from phase I to phase II is the second-kind PT (dark circles on the curve). A similar picture is also observed for $r = 0.9$ and $r = 1.0$, at which transition from phase III to phase II occurs in the system. Within $0.6 \le r \le 0.8$, where transition from phase III to phase II occurs, the first-kind PT is observed (light circles on the curve).

To perform a deeper analysis of a PT kind, a histogram data analysis of the MC method was used. The results of our study show that the transition from the antiferromagnetic phase to the paramagnetic phase is the second-kind PT. This is demonstrated in Figure 18. This figure represents energy distribution histograms for systems with linear dimensions $L = 36, 48$ and 90 for $r = 0.3$. The curves are plotted for $T = T_N$. Figure 19 shows that one clearly defined peak, which grows with increasing linear dimensions of the system, is observed on the dependence of probability $P(U)$ on energy U for all linear dimensions. Such behavior supports the second-kind PT. A similar picture is observed throughout $0.0 \le r \le 0.5$ and for $r = 0.9$.

As or the transition from the superantiferromagnetic phase to the paramagnetic phase, we have found that the first-king PT is observed within $0.6 \le r \le 0.8$. This is shown in Figure 19. This figure represents energy distribution histograms for $r = 0.8$ at various linear dimensions L. The figure shows that two clearly defined peaks, which grow with increasing linear dimensions of the system, are observed on the dependence of probability $P(U)$ on energy U for all linear dimensions. The twin peak on the

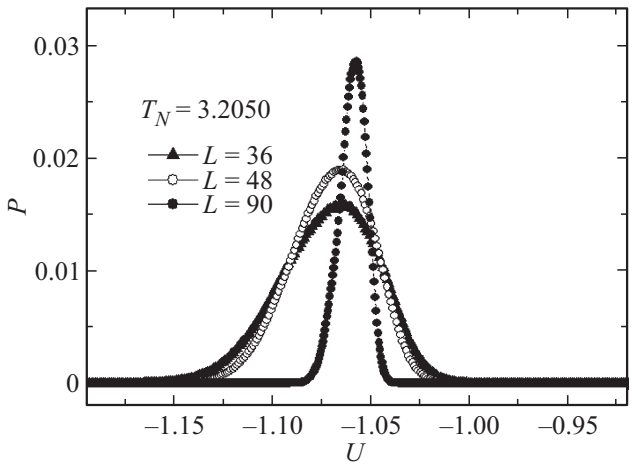

Figure 18. Energy distribution histograms for $r = 0.3$.

Table 2. Critical parameter values for the antiferromagnetic cubic lattice Ising model

r	T_N	ν	α	β	γ	η	$\alpha + 2\beta + \gamma = 2$
Unfrust. Ising model [128]	4.5111(3)	0.6305(25)	0.108(9)	0.3265(25)	1.239(4)	0.037(3)	2
0.0	4.5110(2)	0.630(5)	0.110(5)	0.320(5)	1.241(5)	0.03(1)	1.991
0.1	4.1020(2)	0.625(5)	0.115(5)	0.317(5)	1.238(5)	0.02(1)	1.986
0.2	3.4440(2)	0.633(5)	0.119(5)	0.328(5)	1.237(5)	0.04(1)	2.012
0.3	3.2050(2)	0.624(5)	0.118(5)	0.319(5)	1.243(5)	0.02(1)	1.999
0.4	2.6820(2)	0.632(5)	0.110(5)	0.322(5)	1.245(5)	0.02(1)	1.999
0.9	3.8250(2)	0.550(5)	0.339(5)	0.249(5)	1.188(5)	−0.14(1)	2.025
1.0	4.1730(2)	0.549(5)	0.330(5)	0.245(5)	1.190(5)	−0.16(5)	2
$r = 1.0$ [129]	1.355(2)	0.55(2)	0.33(5)	–	–	−0.28(6)	–
$r = 1.0$ [130]	1.347(1)	0.56(2)	0.32(2)	0.25(2)	–	−0.10(2)	–

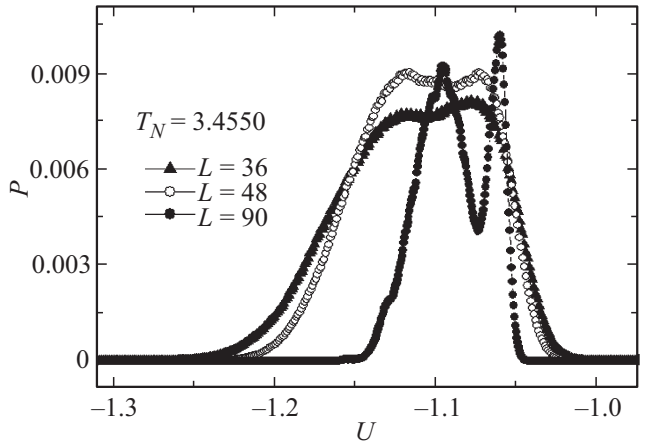

Figure 19. Energy distribution histograms for $r = 0.8$.

energy distribution histogram is indicative of the first-kind PT. A similar picture is observed throughout $0.6 \leq r \leq 0.8$. Analysis of our data shows that consideration of the second-neighbor interactions inside the layers at specific interaction values results in PT change [127].

To calculate the static CI, the FSS theory relations were used. The CI calculation procedure is described in Section 4.1. This procedure was used to calculate CI for the model of interest within $0.0 \leq r \leq 0.5$, and for $r = 0.9$ and 1.0, where the second-kind PT is observed. All static CI values calculated in this way are listed in Table 2 [127].

For $r = 0.5$, the attempt to calculate the critical parameters with the allowable accuracy has failed. We suggest that this is due to the fact that three different phases coexist in this point. Comparison of numerical CI values obtained herein with the literature data shows good agreement, the critical parameters for this model for various r values have been calculated by us for the first time.

As shown in Table 2, the critical temperature TN decreases with increasing next-neighbor interaction up to $r = 0.4$. With further increase in r, the critical temperature starts growing. All CI values calculated by us within $0.0 \leq r \leq 0.4$, coincide within the allowable accuracy with CI values of the three-dimensional unfrustrated Ising model [128]. This indicates that this model within $0.0 \leq r \leq 0.4$ is included in the same critical behavior universality class as the unfrustrated Ising model. CI values calculated by us for $r = 0.9$ and 1.0 well agree with those calculated in [129,130] for the fully frustrated three-dimensional cubic lattice Ising model, but they differ greatly from the data obtained by us for this model within$0.0 \leq r \leq 0.4$. It can be assumed that consideration of the second-neighbor interactions inside the lattice layers for the antiferromagnetic cubic lattice Ising model results in the critical behavior universality class change within $0.8 < r \leq 1.0$. In this case, CI coincide with the data for the fully frustrated three-dimensional cubic lattice Ising model [131,132].

4.4. Triangular layered lattice three-dimensional Ising model

The two-dimensional antiferromagnetic triangular layered lattice Ising model is a relatively simple geometrically frustrated model. In this model where interaction is limited only by the nearest neighbors, the spin ordering is strongly suppressed due to the frustration effects. As a result this system has now PT at any finite temperature [133–135]. Consideration of the second-neighbor interactions in this model plays a significant role and causes various types of long-range order depending on the values and sign of the second-neighbor interaction [136].

Theoretical and numerical investigations of the three-dimensional antiferromagnetic triangular layered lattice Ising model were controversial. Landau–Ginzburg–Wilson theory predicted $3d\,XY$-behavior for the observed magnetic PT [137,138]. Later, the MC simulation gave the results typical for tricritical behavior [139]. Later investigations using the MC histogram method and FSS theory showed the set of CI that differs from the tricritical behavior and is rather close to $3d\,XY$-model [140,141].

The authors of [142] studies the ordered phases and PT in the triangular layered lattice Ising model with strong interlayer interaction. This model may be used to describe $CsCoCl_3$ and $CsCoBr_3$. Calculations carried out for them

within the mean field approximation [143] and by the cluster variation method show that one of three magnetic sublattices is probably disordered.

However, the MC method shows that such partially disordered states are described by the a mode with a randomly space- and time-varying phase [145,146]. These results may explain the observed obvious time fluctuations of the magnetic structure [147].

The MC simulation of the triangular layered lattice Ising antiferromagnet taking into account the antiferromagnetic second-neighbor interactions shows that there is the first-kind PT between the low-temperature two-sublattice antiferromagnetic phase and high-temperature paramagnetic phase. This scenario differs from that observed when the first-neighbor interactions are ferromagnetic. For such case, the Berezinsky–Kosterlitz–Taules pahse in the isolated layers occurs at an intermediate temperature between the three-sublattice ferrimagnetic phase at low temperature and paramagnetic phase at high temperature [148].

As of today, some issues regarding the effect of the interlayer exchange interaction on the Ising antiferromagnet PT are still controversial. The findings obtained for the antiferromagnetic triangular layered lattice Ising model PT with various interlayer exchange interaction values are provided in herein. The antiferromagnetic triangular layered lattice Ising model is described by the Hamiltonian

$$H = -J_1 \sum_{\langle i,j \rangle} (S_i \cdot S_j) - J_2 \sum_{\langle i,l \rangle} (S_i \cdot S_l) - J_3 \sum_{\langle i,k \rangle} (S_i \cdot S_k), \tag{23}$$

where $J_1 < 0$, $J_2 < 0$ and $J_3 > 0$ are the exchange interaction constants. The lattice contains two-dimensional triangular layers folded along the orthogonal axis. The first term in equation (23) characterizes the antiferromagnetic interaction of all nearest neighbors which is assumed equal within the layer, the second term characterizes the interlayer antiferromagnetic interaction and the third term characterizes the ferromagnetic third-neighbor interaction within the layers. For calculations, we assume that $|J_1| = |J_3| = 1$ and change J_2 value. $r = J_2/J_1$ is the interlayer and intralayer exchange relation. $0.01 < r \leq 1.0$ interval is addressed. The investigations were carried out the Wang–Landau algorithm and replete exchange algorithm of the MC method. The calculations were carried out for the systems with PBC and linear dimensions $L \times L \times L = N$, $L = 18-90$.

The order parameter of system m was calculated using expression [149]:

$$m = \frac{3}{N} \sqrt{\langle M_A^2 + M_B^2 + M_C^2 \rangle / 3}, \tag{24}$$

where M_A, M_B and M_C are magnetizations of three sublattices.

To determine the critical temperatures T_N, we used the fourth-order Binder cumulant method U_L. The critical temperatures obtained for the addressed r values are listed in Table 3.

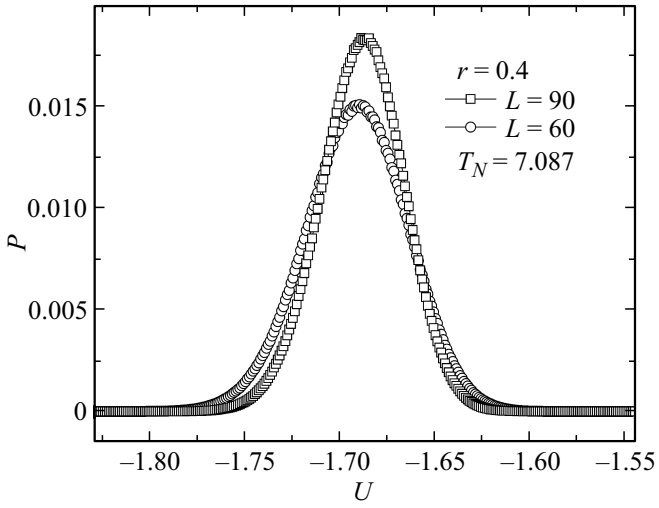

Figure 20. Energy distribution histograms for a system with linear dimensions $L = 60$ and $L = 90$ for $r = 0.4$.

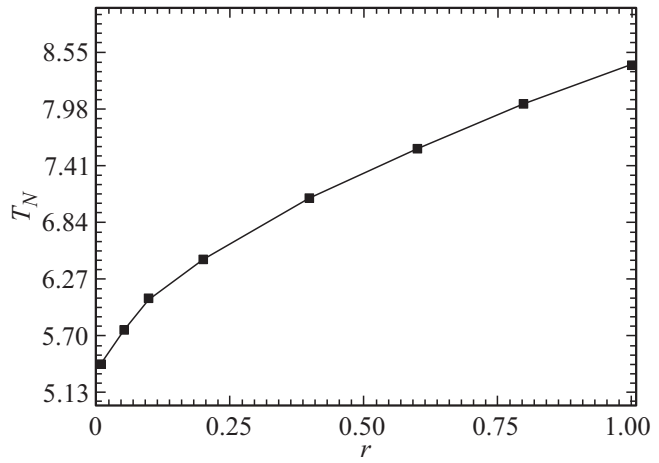

Figure 21. The phase diagram of dependence of the critical temperature on the interlayer exchange interaction for the three-dimensional triangular lattice Ising model.

The PT kind analysis was carried out using the histogram data analysis of the MC method [94,150]. Our findings show that PT for all addressed r values are second-kind transitions. This is demonstrated in Figure 20, where the energy distribution histograms are provided for a system with linear dimensions $L = 60$ and 90 $r = 0.4$. The provided histograms show that the dependence of probability P on energy U has one clearly defined peak, which supports the second-kind PT. The same result has been obtained for all remaining r values.

Figure 21 shows the phase diagram characterizing the dependence of the critical temperature on the interlayer exchange interaction. The diagram shows that decreasing interlayer exchange interaction results in decreasing PT temperature. Analysis of our data shows that the transition from the disordered phase to the ordered phase within the addressed r interval is the second-order PT [151].

Table 3. Critical parameters for the triangular layered lattice Ising model with variable interlayer exchange interaction

r	T_N	ν	α	β	γ	η	$\alpha + 2\beta + \gamma = 2$
0.01	5.420(1)	0.577(15)	0.26(5)	0.284(15)	0.81(5)	0.59(10)	1.6
0.05	5.751(1)	0.592(15)	0.22(5)	0.292(15)	0.88(5)	0.51(10)	1.6
0.1	6.066(1)	0.651(15)	0.05(5)	0.370(15)	1.19(5)	0.16(10)	1.98
0.2	6.465(1)	0.648(15)	0.05(5)	0.365(15)	1.21(5)	0.13(10)	1.99
0.4	7.087(1)	0.660(15)	0.02(5)	0.369(15)	1.20(5)	0.18(10)	1.95
0.6	7.5850(1)	0.648(15)	0.07(5)	0.362(15)	1.17(5)	0.19(10)	1.96
0.8	8.031(1)	0.652(15)	0.05(5)	0.373(15)	1.20(5)	0.15(10)	1.99
1.0	8.427(1)	0.650(15)	0.05(5)	0.370(15)	1.16(5)	0.21(10)	1.95

Table 3 lists the CI values for all addressed r values calculated using the FSS theory relations. The Table shows that the numerical CI values within $0.05 < r \leq 1.0$ coincide with each other within the allowable accuracy. It should be also noted that the scaling relation between CI is satisfied with sufficiently high accuracy. In this case, the CI values within $0.05 < r \leq 1.0$ do not depend on the interlayer interaction and coincide with each other within the allowable accuracy and do not correspond to any known critical behavior universality class. At $r \leq 0.05$, the CI values change considerably and the scaling relations between them are not satisfied any longer. It is suggested that at $r = 0.05$ crossover from the three-dimensional critical behavior to the quasi two-dimensional critical behavior occurs in the system [152,153].

4.5. Body-centered cubic lattice Ising mode

Findings for PT and thermodynamic properties of the antiferromagnetic BCC lattice Ising model taking into account the second-neighbor interaction obtained using the MC replete exchange (REMC) algorithm and Wang–replete (WLA) algorithm are described herein.

Theoretical calculations and MC numerical simulation for the BCC lattice Ising model were described in [154–159]. The theoretical investigations show that the second-kind PT occurs for the simple cubic lattice and BCC lattice Ising model [155–157]. According to [158,159], the second-kind PT changes to the first-kind PT in the system when the second-neighbor interaction increases. Consideration of the second-neighbor in this model interaction can result in frustrations.

The antiferromagnetic BCC lattice Ising model including the first- and second-neighbor interactions is described by the following Hamiltonian [160]:

$$H = -J_1 \sum_{\langle i,j \rangle} (S_i \cdot S_j) - J_2 \sum_{\langle i,l \rangle} (S_i \cdot S_l). \qquad (25)$$

The first term in equation (25) takes into account the first-neighbor exchange interaction ($J_1 < 0$), and the second term takes into account the second-neighbor exchange interaction ($J_2 < 0$). $r = J_2/J_1$ is the second-neighbor interaction. The calculations were carried out for the systems with PBC and linear dimensions $L \times L \times L = N$, $L = 12-90$. The relation of the second- and first-neighbor exchange interactions varied within $0.0 \leq r \leq 1.0$.

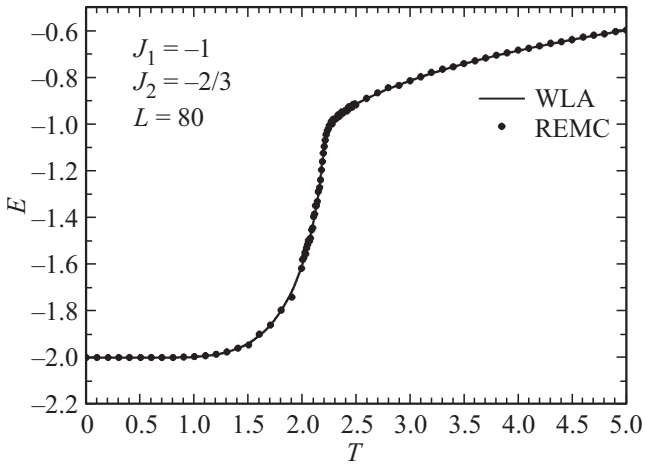

Figure 22. Temperature dependences of energy.

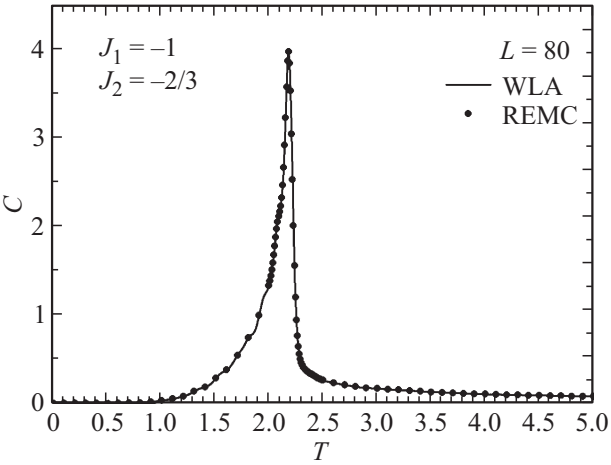

Figure 23. Temperature dependences of heat capacity.

Figures 22 and 23 show the temperature dependences of energy and heat capacity obtained using the replete exchange algorithm and Wang–Landau algorithm. These figures demonstrate that the data obtained using different

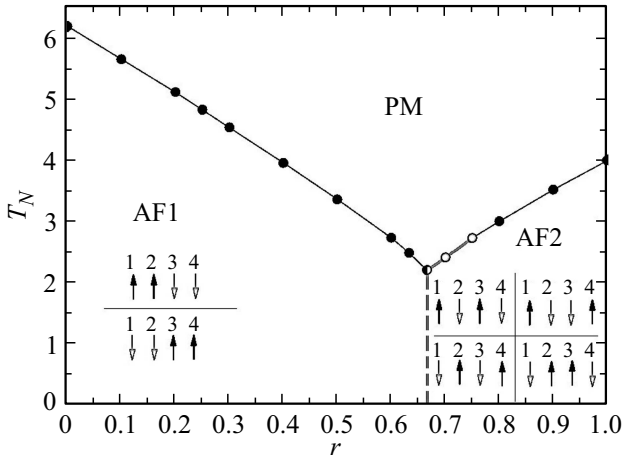

Figure 24. The phase diagram of dependence of the critical temperature on the second-neighbor interaction for the BCC lattice Ising model.

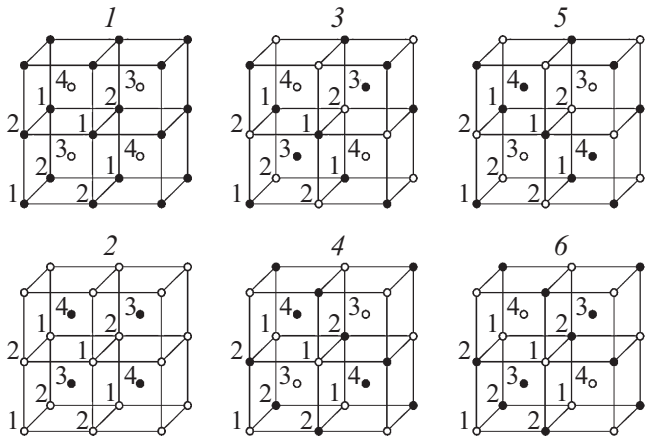

Figure 25. Magnetic structures of the ground state for $r = 2/3$.

algorithms correspond closely to each other. This suggests reliability and accuracy of the findings.

Figure 24 shows the phase diagram of dependence of the critical temperature on the second-neighbor interaction. The diagram shows that three different phases intersect in point $r = 2/3$: AF1 — antiferromagnetic, PM paramagnetic and AF2 2- type antiferromagnetic phase[157,158]. Spin directions in sublattices are shown with arrows on the phase diagram. Figure 25 shows magnetic structures of the ground state for the model of interest for $r = 2/3$, which were obtained using the Wang–Landau algorithm (black and light circles show the spin directions). Numbers *1–6* in this figure indicate all possible magnetic structures of the ground state observed in this model.

Energy state density $g(E)$ for systems with various linear dimensions L is shown in Figure 26. The curve shows that there is no strong ground state degeneracy in this system. This suggests that the first-neighbor and second-neighbor exchange interaction competition in the addressed model does not result in strong ground state degeneracy opposed to the square lattice Ising model [108].

Temperature dependence of entropy S is shown in Figure 27. This figure shows that the system entropy with increasing temperature tends to the theoretically predicted value $\ln 2$. At low temperatures close to the absolute zero, the system entropy tends to a near-zero value. Such entropy behavior also suggests that the ground state degeneracy is not available in this model. It can be assumed that the exchange interaction competition in this model does not cause any frustrations.

For the PT kind analysis, we used the MC histogram data analysis method for the data obtained using both the replete algorithm and Wang–Landau algorithm. It is shown that the second-kind PT is observed within $0.0 \le r \le 0.6$ and $0.8 \le r \le 1.0$, which is fully consistent with [105]. A more detailed investigations of $2/3 \le r \le 0.75$ has shown that the second-kind PT is observed for $r = 2/3$. This is demonstrated in Figure 28. This figure represents energy distribution histograms for a system with linear dimensions

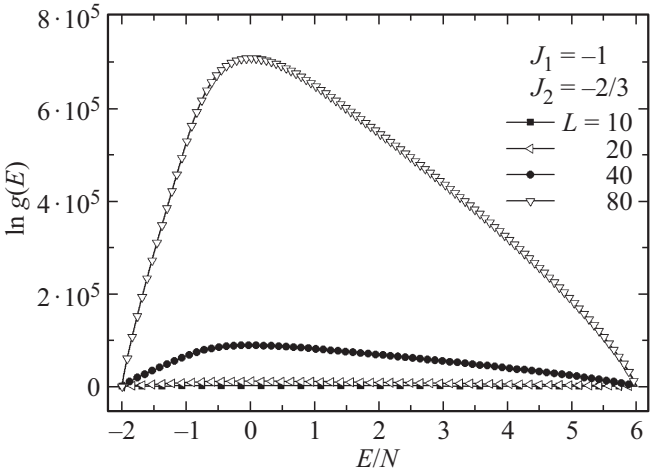

Figure 26. Energy state density $g(E)$ for systems with various linear dimensions L.

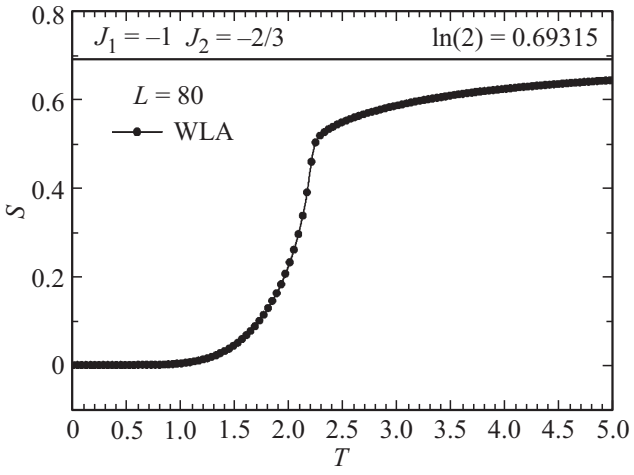

Figure 27. Temperature dependence of entropy.

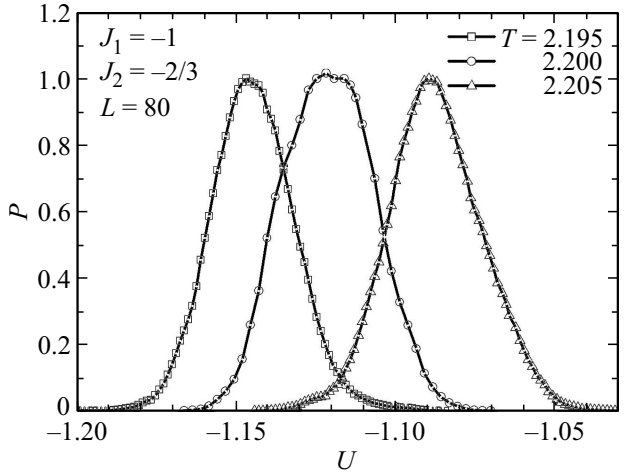

Figure 28. Energy distribution histograms for a system with linear dimensions $L = 80$.

$L = 80$. The curves are built near the critical temperature. The figures show that the dependence of probability $P(U)$ on energy U for all temperatures has one clearly defined peak, which supports the second-kind PT. Thus, the findings show that the phase diagram (Figure 24) contains a narrow region $(2/3 < r \leq 0.75)$ where the transition is implemented as the first-kind PT.

Analysis of this data suggests that consideration of the antiferromagnetic second-neighbor interactions in the antiferromagnetic BCC lattice Ising model results in sixfold degeneracy of the ground state, rather than in frustration. The second-kind PT is observed in the addressed model at $r = 2/3$ [161–165]. The obtained data may be used to describe particular antiferromagnetic BCC lattice materials such as FeCr [166], FeAl, FeCo [167] and some others as described in [168].

5. Ising models with frustrations in the magnetic field

5.1. Triangular lattice Ising model in the magnetic field

An external magnetic field applied to the two-dimensional antiferromagnetic triangular lattice Ising model stabilizes the spin state and induces PT in the system [136]. Opposed to the two-dimensional case, the tree-dimensional antiferromagnetic triangular lattice Ising model is still poorly understood. This model allows to describe a variety of systems, including artificial dipole magnets [169], compounds where electrically charged dumbbells act as the Ising degrees of freedom [170], frustrated Coulomb liquids [171] etc.

Many physical properties of frustrated systems may depend on external factors, for example, magnetic field. Therefore, the study of the three-dimensional antiferromagnetic triangular lattice Ising model provides answers to some questions regarding the impact of magnetic field on PT of layered frustrated spin systems.

The Section provides the findings for PT in the antiferromagnetic triangular layered lattice Ising model in the magnetic field described by the Hamiltonian

$$H = -J_1 \sum_{\langle i,j \rangle} (S_i \cdot S_j) - h \sum_i S_i^z. \qquad (26)$$

The lattice contains two-dimensional triangular layers folded along the orthogonal axis z, h is the external magnetic field oriented along the z axis. The calculations were carried out for the systems with PBC and linear dimensions $L \times L \times L = N$, $L = 12-48$.

Figure 29 shows the temperature dependences of heat capacity obtained for the system with liners dimensions $L = 36$ at various magnetic field strengths h (hereinafter magnetic field is given in terms of $k_B T$). A clearly defined peak is observed in the dependences of heat capacity on temperature within $0 \leq h \leq 6$ near the critical temperature. This peak moves towards low temperatures with increasing magnetic filed strength. There is competition between the internal molecular field that induces antiferromagnetic ordering in the system and the external magnetic field that arranges the system along the field. therefore, with the increasing external magnetic field, PT occurs in the systems at lower temperatures. A small second peak is observed in the low-temperature region. It should be noted that twin peaks are associated with so-called intermediate partially disordered antiferromagnetic phase. The curves show that heat capacity peaks within $6 < h \leq 12$ become more smooth or disappear at all. This is due to the fact that the magnetic field fully suppresses the system fluctuations and PT is degraded in the system.

Figure 30 shows the magnetization vs. magnetic field curve for different temperatures. There is a magnetization plateau equal to 1/3 saturation magnetization. When the

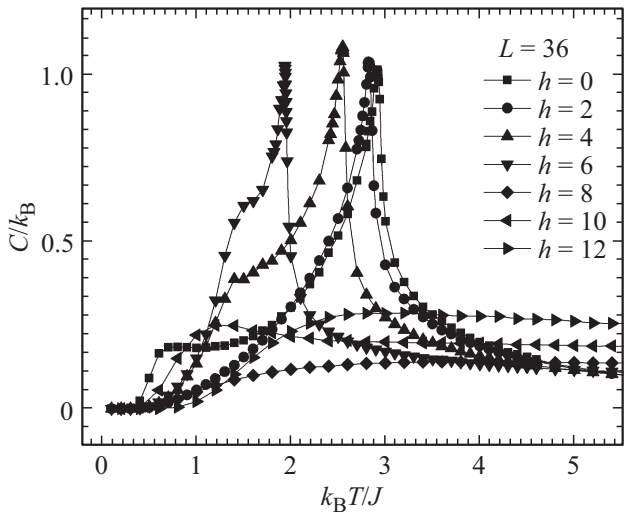

Figure 29. Temperature dependences of heat capacity for different magnetic field strengths h.

external magnetic field is included, the ground state having a long-range order may be represented. In this state, the spins of two sublattices are arranged along the field, while the spins of the third sublattice are oriented opposite to the magnetic field. This induces the magnetization plateau equal to 1/3 saturation magnetization. With the increasing temperature, the plateau gradually disappears and we observe smooth growth of magnetization up to saturation. This is explained by the spin temperature fluctuations.

Figure 31 shows temperature dependences of entropy S at different magnetic field strengths h. According to the theoretical predictions, the entropy for the system of interest shall tend to $\ln 2$ with temperature growth. At low temperatures, the entropy for unfrustrated systems tends to zero, and is non-zero for frustrated systems. The figure shows that the entropy at high temperatures tends to $\ln 2$. At low temperatures, the entropy tends to non-zero values.

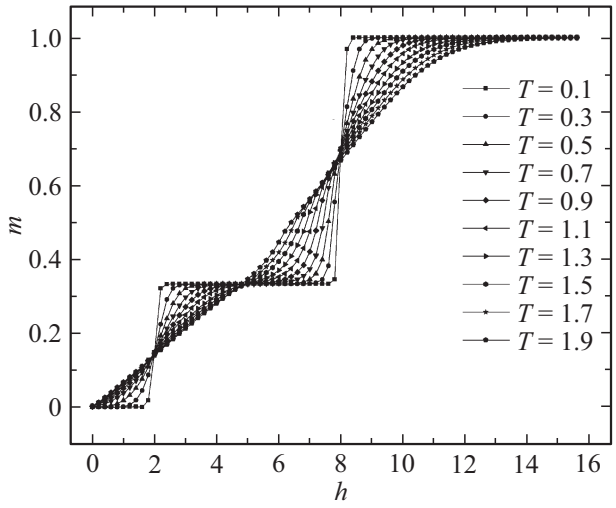

Figure 30. Magnetization dependences on the magnetic field strength for different temperatures.

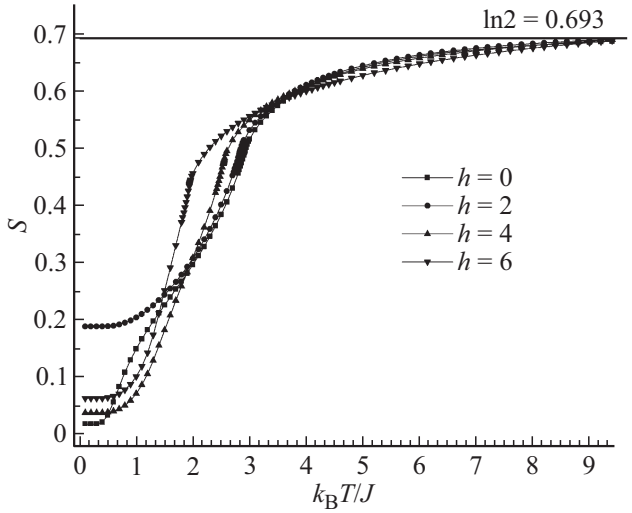

Figure 31. Temperature dependences of entropy S for different magnetic field strengths h.

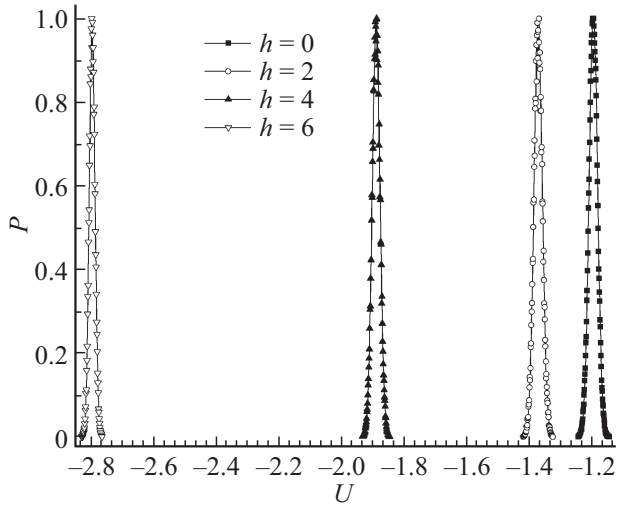

Figure 32. Energy distribution histograms for a system with linear dimensions $L = 36$ at $h = 0, 2, 4, 6$.

With increasing h, growth of the value to which the entropy tends at low temperatures is observed. Such behavior is typical for frustrated spin systems. This suggests that frustration effects are observed in this model at the given magnetic field strengths. For higher fields, the entropy tends to zero at low temperatures and to $\ln 2$ in a high temperature region. It can be claimed that there is no ground state degeneracy in this model at high magnetic field strength and the system achieves the ordered state.

For PT kind analysis, we used the MC histogram data analysis method. Our findings show that PT for the field strengths within $0 \leq h \leq 6$ are the second-kind transitions. This is demonstrated in Figure 32, where the energy distribution histograms are provided for a system with linear dimensions $L = 36$ and 6 $h = 0$, 2, 4 and 6. The curves show that one clearly defined peak is observed on the dependence of probability on energy. One peak on the energy distribution histogram supports the second-kind PT [172–175].

5.2. Body-centered cubic lattice Ising model in magnetic field

The influence of the magnetic field on the nature of PT, magnetic and thermodynamic properties of the antiferromagnetic BCC lattice Ising model taking into account the first- and second-neighbor interactions will be discussed herein.

The Hamiltonian in the antiferromagnetic BCC lattice Ising model taking into account the first- and second-neighbor interaction as well as external magnetic field is written as follows

$$H = -J_1 \sum_{\langle i,j \rangle} (S_i \cdot S_j) - J_2 \sum_{\langle i,l \rangle} (S_i \cdot S_l) - h \sum_{\langle i \rangle} S_i^z, \quad (27)$$

where J_1 and J_2 are the antiferromagnetic exchange interaction constants of the first neighbors $(J_1 < 0)$ and

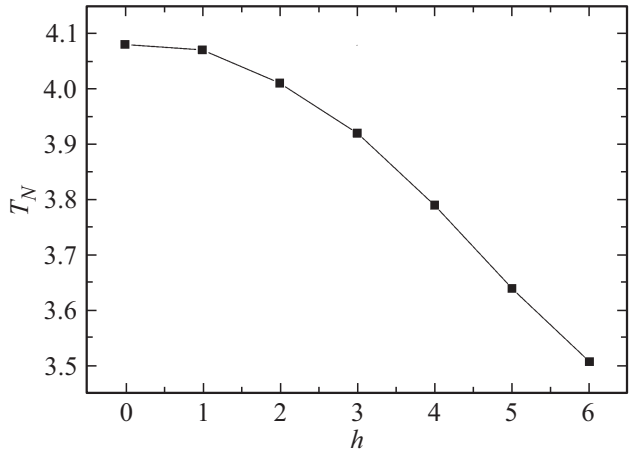

Figure 33. Dependence of the critical temperature on the magnetic field strength h for the BCC lattice Ising model.

second neighbors ($J_2 < 0$), h is the magnetic field strength. Magnetic field is oriented along the z axis. Using the MC replete algorithms, calculations were carried out for the systems with PBC and linear dimensions $2 \times L \times L \times L = N$, $L = 18-90$.

MC histogram data analysis shows that one peak is observed on the energy distribution histograms for all field values within $0.0 \leq h \leq 6.0$. This suggests that the second-kind PT is implemented in he system.

Figure 33 shows the dependence of the critical temperature T_N on the magnetic field strength h. It is shown that T_N decreases with increasing magnetic field strength within $0.0 \leq h \leq 6.0$. Within the addressed magnetic field interval, transition from the antiferromagnetic phase to the paramagnetic phase is implemented as the second-kind PT [176,177]. According to [178], the second-king PT occurs in the magnetic field range $0.0 \leq h \leq 10.0$ and the first-kind PT is observed within $11.0 \leq h \leq 13.0$. Strong magnetic field ($h \geq 14.0$) has been found to result in PT suppression.

6. Conclusion

The data on the frustration effect on phase transitions, critical behavior and thermodynamic properties of the Ising models provided herein suggest that an extremely wide and versatile behavior picture is formed. Occurrence of the frustrated state independently on its cause, whether due to the lattice geometry or competing interactions, may influence phase transitions and critical behavior dramatically. In this case, the kind of phase transition and the critical behavior universality class can be changed, and non-universal critical behavior can be also observed sometimes. Behavior features of frustrated spin systems depend to a great extent on the relation of competing exchange interaction forces, on the type of lattice and on the space dimension. Simultaneous influence of all these factors results in extreme versatility of phase diagrams of such systems.

Funding

The study was partially supported by NCFM's research program („Investigations of strong and superstrong magnetic field" project).

Conflict of interest

The authors declare that they have no conflict of interest.

References

[1] W. Lenz. Z. Phys. **21**, 613 (1920).
[2] E. Ising. Z. Phys. **31**, 253 (1925).
[3] L. Onsager. Phys. Rev. **65**, 117 (1944).
[4] T.D. Lee, C.N. Yang. Phys. Rev. **87**, 410 (1952).
[5] J.C. Wheeler. Ann. Rev. Phys. Chem. **28**, 411 (1977).
[6] M. Blume, V.J. Emery, R.B. Griffiths. Phys. Rev. A **4**, 1071 (1971).
[7] C.J. Thompson. Biopolymers **6**, 1101 (1968).
[8] S. Torquatto. Phys. Biol. **8**, 015017 (2011).
[9] E. Alvarez-Lacalle, B. Echebarria, J. Spalding, Y. Shiferaw. Phys. Rev. Lett. **114**, 108101 (2015).
[10] A. Mailhot, M.L. Plumer, A. Caille. Phys. Rev. B **50**, 6854 (1994-II).
[11] K. Binder, E. Luijten. Phys. Rep. **344**, 179 (2001).
[12] D.P. Landau. Physica A **205**, 41 (1994).
[13] I.P. Beloborov, R.S. Gekht, V.A. Ignatchenko. ZhETF **84**, 1097 (1983). (in Russian).
[14] D. Loison, A.I. Sokolov, B. Delamotte, S.A. Antonenko, K.D. Schotte, H.T. Diep. JETP Lett. **72**, 337 (2000).
[15] J. Snyder, J.S. Slusky, R.J. Cava, P. Schiffer. Nature **413**, 48 (2001).
[16] J.S. Gardner, A. Keren, G. Ehlers, C. Stock, Eva Segal, J.M. Roper, B. Fåk, M.B. Stone, P.R. Hammar, D.H. Reich, B.D. Gaulin. Phys. Rev. B **68**, 180401 (2003).
[17] G. Möller, R. Moessner. Phys. Rev. Lett. **96**, 237202 (2006).
[18] F.A. Kassan-Ogly, B.N. Filippov, A.K. Murtazaev, M.K. Ramazanov, M.K. Badiev. JMMM **324**, 3418 (2012).
[19] S.E. Korshunov. UFN, **176**, 233 (2006). (in Russian).
[20] R. Baxter. Tochno reshaemye modeli v statisticheskoy mekhanike / Pod red. A.M. Brodskogo. Mir, M., (1985). 486 p. (in Russian).
[21] L.D. Fosdik. Bull. Am. Phys. Soc. **2**, 239 (1957).
[22] D.P. Landau. Phys. Rev. B **13**, 2997 (1976).
[23] D.P. Landau. Phys. Rev. B **14**, 255 (1976).
[24] D.P. Landau. Phys. Rev. B **16**, 4164 (1977).
[25] K. Binder. Phys. Status Solidi B **46**, 567 (1971).
[26] L. Hua, J.W. Tucker. JMMM **140–144**, 1509 (1995).
[27] D. Farsal, M. Snina, M. Bennai, M. Badia. J. Supercond. Nov. Magn. **30**, 2187 (2017).
[28] D. Farsal, M. Bennai, M. Badia. SPIN **8**, 1850010 (2018).
[29] T. Balcerzak, K. Szałowski, A. Bobák, M. Žukovič. Phys. Rev. E **98**, 022123 (2018).
[30] Y. Aoyama, W. Chen, M. Tanaka. J. Phys. Soc. Jpn. **66**, 272 (1997).
[31] M.E.J. Newman, G.T. Barkema. Phys. Rev. E **53**, 393 (1996).

[32] E.T. Gawlinski, S. Kumar, M. Grant, J.D. Gunton, K. Kaski. Phys. Rev. B **32**, 1575 (1985).
[33] C. Dekker, B.J. Dikken, A.F.M. Arts. Solid State Commun. **54**, 887 (1985).
[34] J.D. Shore, G.M. Thurston. Phys. Rev. E **92**, 062123 (2015).
[35] H.-J. Wu, W. Wang, B.-C. Li, Q. Li, J.-H. Xu, F. Wang. J. Phys. Chem. Solids **136**, 109174 (2020).
[36] O. Nagai, Y. Yamada, K. Nishino, Y. Miyatake. Phys. Rev. B **35**, 3425 (1987).
[37] R. Bidaux, N. Boccara. Phys. Rev. B **34**, 4881 (1986).
[38] M. Danino. Solid State Commun. **52**, 885 (1984).
[39] S.N. Coppersmith. Phys. Rev. B **32**, 1594 (1985).
[40] J.D. Kimel, S. Black, P. Carter, Y.L. Wang. Phys. Rev. B **35**, 3347 (1987).
[41] S.V. Belim, I.B. Larionov. Vestn. Moskovsk. un-ta. Ser. 3. Fizika. Astronomiya, **4** (58), (2018). (in Russian).
[42] T. Arh, B. Sana, M. Pregelj, P. Khuntia, Z. Jagličić, M.D. Le, P.K. Biswas, P. Manuel, L. Mangin-Thro, A. Ozarowski, A. Zorko. Nature Mater. **21**, 416 (2022).
[43] K. Dutta, D. Talukdar. JMMM **556**, 169344 (2022).
[44] Y. Shokef, A. Souslov, T.C. Lubensky. Proc. Natl. Acad. Sci. U.S.A. (PNAS) **108**, 11804 (2011).
[45] W. Kerler, P. Rehberg. Phys. Rev. B **49**, 9688 (1994).
[46] A.K. Murtazaev, I.K. kamilov, M.K. Ramazanov. FTT, **47**, 1125 (2005). (in Russian).
[47] M. Schmidt, G.L. Kohlrausch, F.M. Zimmer. Physica A **596**, 127126 (2022).
[48] E. Jurčišinová, M. Jurčišin. Physica A **603**, 127731 (2022).
[49] R.M. Liu, W.Z. Zhuo, X.B. Lu, X.S. Gao, M.H. Qin, J.-M. Liu, S. Dong. Phys. Rev. E **93**, 032114 (2016).
[50] R. Moessner, S.L. Sondhi. Phys. Rev. B **63**, 224401 (2001).
[51] A.G. Cavaliere, A. Pelissetto. J. Phys. A **52**, 174002 (2019).
[52] D.N. Yasinskaya, V.A. Ulitko, Yu.D. Panov. FTT, **63**, 1350 (2021). (in Russian).
[53] E. Jurčišinová, M. Jurčišin. Phys. Rev. E **104**, 044121 (2021).
[54] E.S. Tsuvarev, F.A. Kassan-Ogly, A.I. Proshkin. ZhETF **158**, 504 (2020). (in Russian).
[55] J. Wu, D.C. Mattis. Phys. Rev. B **67**, 224414 (2003).
[56] T. Yoshioka, A. Koga, N. Kawakami. J. Phys. Soc. Jpn. **73**, 1805 (2004).
[57] N. De La Espriella, G.M. Buendía, J.C. Madera. J. Phys. Commun. **2**, 025006 (2018).
[58] H. Bouda, L. Bahmad, R. Masrour, A. Benyoussef. J. Supercond. Nov. Magn. **32**, 1837 (2019).
[59] A. Jabar, R. Masrour. Physica A **515**, 270 (2019).
[60] R. Masrour, A. Jabar. Physica A **539**, 122878 (2020).
[61] E. Jurčišinová, M. Jurčišin. Phys. Rev. B **101**, 214443 (2020).
[62] E. Jurčišinová, M. Jurčišin. Physica A **583**, 126338 (2021).
[63] E. Jurčišinová, M. Jurčišin. Phys. Lett. A **388**, 127043 (2021).
[64] S.V. Belim, I.B. Larionov, R.V. Solonetsky. Fizika metallov i metallovedenie, **117**, 1115 (2016). (in Russian).
[65] P.F. Godoy, M. Schmidt, M.F. Zimmer. Phys. Lett. A **384**, 126687 (2020).
[66] H. Li, L.-P. Yang. Phys. Rev. E **104**, 024118 (2021).
[67] A.O. Sorokin. Physica A **602**, 127621 (2022).
[68] Y. Hu, P. Charbonneau. Phys. Rev. B **104**, 144429 (2021).
[69] A.V. Zarubin, F.A. Kassan-Ogly, A.I. Proshkin. JMMM **514**, 167144 (2020).
[70] F.A. Kassan-Ogly, A.I. Proshkin. Phys. Met. Metallogr. **120**, 1359 (2019).
[71] A.I. Proshkin, F.A. Kassan-Ogly. Phys. Met. Metallogr **120**, 1366 (2019).
[72] G. Toulouse. Commun. Phys. **2**, 115 (1977).
[73] V.S. Dotsenko. UFN, **163**, 1 (1993). (in Russian).
[74] A.P. Ramirez. Annu. Rev. Mater. Sci. **24**, 453 (1994).
[75] V.S. Dotsenko. UFN **165**, 481 (1995). (in Russian).
[76] I.K. Kamilov, A.K. Murtazaev, Kh.K. Aliev. UFN, **169**, 773 (1999). (in Russian).
[77] K. Binder. Metody Monte-Carlo v statisticheskoy fizike / Pod. red. G.I. Marchuk, G.A. Mikhailov. Mir, M., (1982). 400 p. (in Russian).
[78] A. Mitsutake, Y. Sugita, Y. Okamoto. Biopolymers (Peptide Science) **60**, 96 (2001).
[79] F. Wang, D.P. Landau. Phys. Rev. Lett. **86**, 2015 (2001).
[80] M.N. Barber. J. Phys. A **12**, 679 (1979).
[81] D.P. Landau, K. Binder. Phys. Rev. B **31**, 5946 (1985).
[82] J.A. Plascak. Physica A **183**, 563 (1992).
[83] D.P. Landau, K. Binder. Monte Carlo Simulations in Statistical Physics. Cambridge University Press, Cambridge (2000).
[84] M.P. Nightingale. Phys. Lett. A **59**, 486 (1977).
[85] R. H. Swendsen, S. Krinsky. Phys. Rev. Lett. **43**, 177 (1979).
[86] K. Binder, D.P. Landau. Phys. Rev. B **21**, 1941 (1980).
[87] K. Minami, M. Suzuki. J. Phys. A **27**, 7301 (1994).
[88] J.L. Morıan-Lıopez, F. Aguilera-Granja, J.M. Sanchez. Phys. Rev. B **48**, 3519 (1993).
[89] J.L. Moran-Lopez, F. Aguilera-Granja, J.M. Sanchez. J. Phys.: Condens. Matter **6**, 9759 (1994).
[90] E. Lopez-Sandoval, J.L. Moran-Lopez, F. Aguilera-Granja. Solid State Commun. **112**, 437 (1999).
[91] C. Buzano, M. Pretti. Phys. Rev. B **56**, 636 (1997).
[92] A.K. Murtazaev, M.K. Ramazanov, M.K. Badiyev, FNT **37**, 1258 (2011). (in Russian)
[93] K. Binder, J.-Sh. Wang. J. Status Phys. **55**, 87 (1989).
[94] Junqi Yin, D.P. Landau. Phys. Rev. E **80**, 051117 (2009).
[95] K. Bimder, D.V. Kheerman. Modelirovanie metodom Monte-Carlo v statisticheskoy fizike. Nauka, M., (1995). (in Russian).
[96] A.R. Anjos, J.R. Viana, J.R. Sousa. Phys. Lett. A **372**, 1180 (2008).
[97] A. Kalz, A. Honecker. Phys. Rev. B **86**, 134410 (2012).
[98] S. Jin, A. Sen, A.W. Sandvik. Phys. Rev. Lett. **108**, 045702 (2012).
[99] A.E. Ferdinand, M.E. Fisher. Phys. Rev. **185**, 832 (1969).
[100] M.E. Fisher, M.N. Barber. Phys. Rev. Lett. **28**, 1516 (1972).
[101] P. Peczak, A.M. Ferrenberg, D.P. Landau. Phys. Rev. B **43**, 6087 (1991).
[102] D. Staufer, A. Aharony. Introduction to Percolation Theory. Taylor & Francis, London (1994).
[103] A.K. Murtazaev, I.K.Kamilov, M.K. Ramazanov. FNT **32**, 323 (2006). (in Russian).
[104] A.K. Murtazaev, M.K. Ramazanov. Phys. Rev. B **76**, 174421 (2007).
[105] Ch. Holm, W. Janke. Phys. Rev. B **48**, 936 (1993).
[106] A. Malakis, P. Kalozoumis, N. Tyraskis. Eur. Phys. J. B **50**, 63 (2006).
[107] A.K. Murtazaev, M.K. Ramazanov, F.A. Kassan-Ogly, M.K. Badiyev, ZhETF **144**, 1239 (2013). (in Russian).
[108] F.A. Kassan-Ogly, A.K. Murtazaev, A.K. Zhuravlev, M.K. Ramazanov, A.I. Proshkin. JMMM **384**, 247 (2015).
[109] A.K. Murtazaev, M.K. Ramazanov, M.K. Badiev. Physica B: Condens. Matter **476**, 1 (2015).
[110] M.K. Ramazanov, A.K. Murtazaev, M.A. Magomedov. Solid State Commun. **233**, 35 (2016).
[111] P. Chandra, P. Coleman, I. Ritchey. J. de Physique **33**, 591 (1993).

[112] J.T. Chalker, P.C.W. Holdsworth, E.F. Shender. Phys. Rev. Lett. **68**, 855 (1992).
[113] A.B. Harris, C. Kallin, A.J. Berlinsky. Phys. Rev. B **45**, 2899 (1992).
[114] R.S. Gekht, I.N. Bondarenko. ZhETF **113**, 2209 (1998). (in Russian).
[115] M. Wolf, K.D. Schotte. J. Phys. A **21**, 2195 (1988).
[116] R.S. Gekht, V.I. Ponomarev. Phase Transitions **20**, 27 (1990).
[117] M. Stahn, R.E. Lechner, H. Dachs, H.E. Jacobs. J. Phys. C **16**, 5073 (1983).
[118] M.G. Townsend, G. Longworth, E. Roudaut. Phys. Rev. B **33**, 4919 (1986).
[119] T. Matsuo, H. Suga. Rev. Inorg. Chem. **3**, 371 (1981).
[120] M. Takano, T. Shinjo, T. Takada. J. Phys. Soc. Jpn. **30**, 1049 (1971).
[121] T. Takagi, M. Mekata. J. Phys. Soc. Jpn. **62**, 3943 (1993).
[122] M.K. Ramazanov. Pis'ma v ZhETF **94** (335), (2011). (in Russian).
[123] M.K. Ramazanov, A.K. Murtazaev, M.A. Magomedov, M.K. Badiev. Phase Transitions **91**, 610 (2018).
[124] A.R. Anjos, J.R. Viana, J.R. de Sousa, J.A. Plascak. Phys. Rev. E **76**, 022103 (2007).
[125] D.R.O. Salmon, N. Crokidakis, A.M. Neto, T.I. Padilha, J.R. Viana, J.R. de Sousa. Int. J. Mod. Phys. B **27**, 1350162 (2013).
[126] M.K. Ramazanov, A.K. Murtazaev. Pis'ma v ZhETF **101** 793 (2015). (in Russian).
[127] M.K. Ramazanov, A.K. Murtazaev. Pis'ma v ZhETF **103** 522 (2016). (in Russian).
[128] J.C. Le Guillou, J. Zinn-Justin. Phys. Rev. B **21**, 3976 (1980).
[129] H.T. Diep, P. Lallemand, O. Nagai. J. Phys. C **18**, 1067 (1985).
[130] L.W. Bernardi, K. Hukushima, H. Takayama. J. Phys. A **32**, 1787 (1999).
[131] M.K. Ramazanov, A.K. Murtazaev. FTT, **59**, 1797 (2017). (in Russian).
[132] M.K. Ramazanov, A.K. Murtazaev. Phase Transitions **91**, 83 (2018).
[133] G.H. Wannier. Phys. Rev. **79**, 357 (1950).
[134] G.F. Newell. Phys. Rev. **79**, 876 (1950).
[135] R.M.F. Houtapel. Physica **16**, 425 (1950).
[136] J. Hose, K. Kadanoff, S. Kirkpatricks, D.R. Nelson. Physica **16**, 1217 (1977).
[137] D. Blankschtein, M. Ma, A. N. Berker, G.S. Grest, C.M. Soukoulis. Phys. Rev. B **29**, 5250 (1984).
[138] G.A. Baker, Jr., B.G. Nickel, D.I. Meiron. Phys. Rev. B **17**, 1365 (1978).
[139] O. Heinonen, R.G. Petschek. Phys. Rev. B **40**, 9052 (1989).
[140] M.L. Plumer, A. Mailhot, R. Ducharme, A. Caille, H.T. Diep. Phys. Rev. B **47**, 312 (1993).
[141] A. Bunker, B.D. Gaulin, C. Kallin. Phys. Rev. B **48**, 15 861 (1993).
[142] N. Todoroki, S. Miyashita. J. Phys. Soc. Jpn. **73**, 412 (2004).
[143] H. Shiba. Prog. Teor. Phys. **64**, 466 (1980).
[144] M. Kaburagi, T. Tonegawa, J. Kanamori. J. Phys. Soc. Jpn. **51**, 3857 (1982).
[145] P. Matsubara, S. Ikeda. Phys. Rev. B **28**, 4064 (1983).
[146] P. Matsubara, S. Inawashira. J. Phys. Soc. Jpn. **53**, 4373 (1984).
[147] H. Yoshizawa, K. Hirakawa. J. Phys. Soc. Jpn. **46**, 448 (1980).
[148] E. Rastelli, S. Regina, A. Tassi. Phys. Rev. **71**, 174406 (2005).
[149] A.K. Murtazaev, M.K. Ramazanov, M.K. Badiev. Physica A **507**, 210 (2018).
[150] F. Wang, D.P. Landau. Phys. Rev. E **64**, 056101 (2001).
[151] A.K. Murtazaev, M.K. Ramazanov, M.K. Badiyev. FNT **45**, 1493 (2019).
[152] A.K. Murtazaev, M.K. Ramazanov, M.K. Badiyev. FTT, **61**, 1898 (2019). (in Russian).
[153] M.K. Badiyev, A.K. Murtazaev, M.K. Ramazanov. ZhETF **150**, 722 (2016). (in Russian).
[154] P.H. Lundow, K. Markstrom, A. Rosengren. Phil. Mag. **89**, 2042 (2009).
[155] P. Butera, M. Comi. Phys. Rev. B **65**, 144431 (2002).
[156] P. Butera, M. Comi. Phys. Rev. B **72**, 014442 (2005).
[157] M. Plischke, J. Oitmaa. Phys. Rev. B **19**, 487 (1979).
[158] J.R. Banavar, D. Jasnow, D.P. Landau. Phys. Rev. B **20**, 3820 (1979).
[159] M.J. Velgakis, M. Ferer. Phys. Rev. B **27**, 401 (1983).
[160] A.K. Murtazaev, M.K. Ramazanov, F.A. Kassan-Ogly, D.R. Kurbanova. ZhETF **147**, 127 (2015). (in Russian).
[161] A.K. Murtazaev, M.K. Ramazanov, D.R. Kurbanova, M.K. Badiev, Ya.K. Abuev. FTT, **59**, 1082 (2017). (in Russian).
[162] A.K. Murtazaev, M.K. Ramazanov, M.A. Magomedov, D.R. Kurbanova. FTT, **60**, 1798 (2018). (in Russian).
[163] A.K. Murtazaev, M.A. Magomedov, M.K. Ramazanov. Pis'ma v ZhETF **107**, 265 (2018). (in Russian).
[164] A.K. Murtazaev, M.K. Ramazanov, D.R. Kurbanova, M.A. Magomedov, K.Sh. Murtazaev. Mater.Lett. **236**, 669 (2019).
[165] Y.-H. Song, Y. Kim, N. Li, B.-N. Lu, R. He, D. Lee. Phys. Rev. C **104**, 044304 (2021).
[166] M.Yu. Lavrentiev, D. Nguyen-Manh, S.L. Dudarev. Phys. Rev. B **81**, 184202 (2010).
[167] R. Leidl, H.W. Diehl. Phys. Rev. B **57**, 1908 (1998).
[168] P. Villars, K. Cenzual, R. Gladyshevskii. Handbook of inorganic substances. Berlin (2017). P. 1955.
[169] E. Mengotti, L.J. Heyderman, A. Bisig, A. Fraile Rodr´łguez, L. Le Guyader, F. Nolting, H.B. Braun. J. Appl. Phys. **105**, 113113 (2009).
[170] A. Smerald, F. Mila. Phys. Rev. Lett. **115**, 147202 (2015).
[171] S. Mahmoudian, L. Rademaker, A. Ralko, S. Fratini, V. Dobrosavljevic. Phys. Rev. Lett. **115**, 025701 (2015).
[172] A.K. Murtazaev, M.K. Badiev, M.K. Ramazanov, M.A. Magomedov. Physica A **555**, 124530 (2020).
[173] M.K. Badiyev, A.K. Murtazaev, M.K. Ramazanov, M.A. Magomedov. FNT **46**, 824 (2020). (in Russian).
[174] A.K. Murtazaev, M.A. Magomedov, M.K. Ramazanov, M.K. Badiev. Physica E **142**, 115320 (2022).
[175] M.K. Badiyev, A.K. Murtazaev, M.K. Ramazanov, M.A. Magomedov. ZhETF **161**, 753 (2022). (in Russian).
[176] A.K. Murtazaev, M.K. Ramazanov, K.Sh. Murtazaev, M.A. Magomedov, M.K. Badiev. FTT, **62**, 229 (2020). (in Russian).
[177] K.S. Murtazaev, A.K. Murtazaev, M.K. Ramazanov, M.A. Magomedov, A.A. Murtazaeva. Low Temperature Phys. **47**, 515 (2021).
[178] K.S. Murtazaev, M.A. Magomedov, A.K. Murtazaev, M.K. Ramazanov. Physica E **148**, 115646 (2023).

Translated by E.Ilyinskaya